Chapter 2.8.5

POLARISED NEUTRON SCATTERING

B. Roessli
Laboratory for Neutron Scattering,
ETH Zürich and Paul Scherrer Institute,
CH-5232 Villigen PSI,
Switzerland

P. Böni
Physik-Department E21,
Technische Universität München,
D-85748 Garching,
Germany

PART 2 SCATTERING IN MICROSCOPIC PHYSICS AND CHEMICAL PHYSICS

Topic 2.8 Neutron Scattering

Contents

§ 1. Introduction

In the previous chapters of this book, experimental results and the theory of elastic and inelastic neutron scattering have been presented under the assumption that the magnetic moments of the neutrons are randomly oriented. It has been shown that details about the physical properties of a system are extracted by analysing the momentum and the energy of the scattered neutrons. It is intuitively imaginable, however, that measuring the spin state of the neutron after scattering relative to its state before the scattering process should provide us with additional information. To that end the cross sections for neutron scattering must now also take into account the relationship between the spin of the neutron with the physical properties of the target.

The polarisation of a neutron is defined as

$$\mathbb{P} = 2\langle \hat{s} \rangle = \langle \hat{\sigma} \rangle, \tag{1}$$

where $\hat{\sigma}$ are the Pauli matrices. Clearly, $|\mathbb{P}|$ is equal to 0 for a completely unpolarised beam and $|\mathbb{P}| = 1$ if the beam is totally polarised. For intermediate values, the neutron beam is not in a well-defined state and the spin part of the neutron wave function must be described by a more general form $\chi = u\chi_\uparrow + v\chi_\downarrow$ with $|u|^2 + |v|^2 = 1$. That is, $|u|^2$ and $|v|^2$ are the probabilities that the neutron spin will be *up* or *down*, respectively. If a matrix operator $\hat{\rho}$ is defined like

$$\hat{\rho} = \chi\chi^\dagger = \begin{pmatrix} |u|^2 & uv^\dagger \\ vu^\dagger & |v|^2 \end{pmatrix} = \frac{1}{2}\left(\mathbb{1} + \mathbf{P}\cdot\hat{\sigma}\right), \tag{2}$$

then the polarisation of the neutron is described by a three-dimensional *vector* with components $\mathbf{P} = (2\Re(u^\dagger v), 2\Im(u^\dagger v), |u|^2 - |v|^2)$ (Lovesey, 1984). The polarisation of a neutron beam is accordingly defined as $\mathbf{P} = \frac{1}{N}\sum \mathbf{P}_j$, where N is the total number of neutrons and the sum runs over the polarisation vector of the individual neutrons j.

The cross section σ and the polarisation of the scattered beam $\mathbf{P}_f$ can be expressed as a function of the density matrix $\hat{\rho}$, the polarisation vector of the incident neutrons $\mathbf{P}_i$ and the interaction potential $\hat{v}$ between the target and the neutron. In its most general form, $\mathbf{P}_f = \mathrm{Tr}\,\hat{\rho}\hat{v}^\dagger\hat{\sigma}\hat{v}/\mathrm{Tr}\,\hat{\rho}\hat{v}^\dagger\hat{v}$.

Neutron scattering with polarised neutrons has been used in fundamental and condensed matter physics for many years despite the low flux of polarised beams. One of the first applications was the study of spin density distributions in ferromagnets, following the pioneering work of Nathans *et al.* (1959). In those days the polarisation of the scattered neutrons was established by measuring their transmission through a magnetised block of iron. As predicted by Halpern and Johnson (1939) the polarisation of the scattered neutrons, $\mathbf{P}_f$, depends on the orientation of the scattering vector $\mathbf{Q}$ with respect to the polarisation of the incident neutrons, $\mathbf{P}_i$, like

$$\mathbf{P}_f = -\hat{\mathbf{Q}}(\hat{\mathbf{Q}} \cdot \mathbf{P}_i), \tag{3}$$

where $\hat{\mathbf{Q}} = \mathbf{Q}/|\mathbf{Q}|$. In other words for $\mathbf{P}_i \parallel \mathbf{Q}$ all magnetic scattering is spin flip. Therefore polarisation analysis in neutron scattering provides an excellent method for distinguishing between nuclear and magnetic scattering. In 1969 the classic paper by Moon *et al.* (Moon *et al.*, 1969) appeared that explains in simple terms one-dimensional **polarisation analysis** (nowadays called longitudinal polarimetry) of neutrons for elastic as well as inelastic neutron scattering. They demonstrated the polarisation dependence of nuclear and magnetic scattering.

Another, rather different application of polarised neutrons is their use for attaining extremely high energy resolution by measuring changes in the neutron beam polarisation caused by inelastic scattering. In 1972, Mezei (Mezei, 1972) suggested using the precession of the magnetic moment of the neutrons in a magnetic field as an internal clock. By means of the so-called *neutron spin-echo* technique energy resolutions on the order of nanoelectronvolts can be achieved, enabling the investigation of slow dynamics, for example, in the critical region of magnetic systems or in polymers and glasses.

Nowadays, polarised neutron scattering is a fast-developing experimental method that finds applications in various fields of condensed-matter research. Examples are

- determination of magnetic structures and spin densities,
- identification of magnetic fluctuations and their different modes and
- separation of coherent from incoherent processes.

In the following, necessarily incomplete sections, we shall provide a presentation of the polarisation dependence of neutron cross sections and show how the different scattering processes can influence the polarisation of the neutron beams. We will then explain how polarised neutron beams can be produced and the polarisation determined after scattering. Finally we shall give examples where the technique of polarised neutron scattering can provide new insight into physical processes in condensed matter research. For a more detailed introduction into the field of polarised neutron scattering, we refer the interested reader to the book of Williams (1988).

§ 2. Elastic Neutron Scattering Cross Section for Polarised Neutrons

The theory of elastic neutron scattering taking into account polarisation effects was derived by Blume (1963). The complete description of the scattering process involving both nuclear and magnetic interactions can be given by means of two master equations. The first one gives the total neutron cross section that depends on the polarisation $\mathbf{P}_i$ of the incident neutron beam as

$$\sigma = NN^* + \mathbf{D}_\perp \cdot \mathbf{D}_\perp^* + \mathbf{P}_i(\mathbf{D}_\perp N^* + \mathbf{D}_\perp^* N) + i\mathbf{P}_i(\mathbf{D}_\perp^* \times \mathbf{D}_\perp), \tag{4}$$

where σ is the total cross section expressed in barns. For simplicity, the contribution of the nuclear spins is neglected. $N = N(\mathbf{Q}) = \sum_i b_i \exp(i\mathbf{Q} \cdot \mathbf{r}_i)$ is the structure factor of the atomic structure that depends on the scattering vector $\mathbf{Q}$ and the scattering lengths of the individual nuclei b_i; $\mathbf{D}_\perp$ is the magnetic interaction vector with $\mathbf{D}_\perp = \mathbf{D}_\perp(\mathbf{Q}) = \hat{\mathbf{Q}} \times (\rho(\mathbf{Q}) \times \hat{\mathbf{Q}})$. $\rho(\mathbf{Q})$ is the Fourier transform of the **magnetic moment distribution** and $\hat{\mathbf{Q}} = \mathbf{Q}/|\mathbf{Q}|$. Therefore, only magnetic components perpendicular to the scattering vector participate in the scattering process. The scalar of the polarisation vector $\mathbf{P}_i$ reflects the degree of polarisation of the neutrons, being equal to ± 1 for a fully polarised beam.

Equation (4) shows that the neutron cross section depends only on the square of the chemical and magnetic structure factor if a nonpolarised neutron beam ($\mathbf{P}_i = 0$) is used. For a fully polarised beam ($|\mathbf{P}_i| = 1$), two additional terms contribute to the scattering, namely the *magnetic–nuclear interference* term and the *chiral* term, respectively. The magnetic–nuclear interference term being proportional to $\mathbf{D}_\perp N^* + \mathbf{D}_\perp^* N$ yields only a nonvanishing contribution to the neutron cross section if a Bragg reflection is due to nuclear and magnetic scattering, like in ferromagnets and in noncentrosymmetric antiferromagnets with propagation vector $\mathbf{Q}_0 = 0$. The chiral term $\mathbf{D}_\perp^* \times \mathbf{D}_\perp$ is nonzero whenever $\mathbf{D}_\perp$ is not parallel to $\mathbf{D}_\perp^*$, as is the case, e.g., for a helicoidal magnetic structure.

The second master equation provides the polarisation of the neutron beam *after* the scattering process relative to the polarisation of the incident neutron beam,

$$\begin{aligned}\mathbf{P}_f\sigma = {} & \mathbf{P}_i NN^* + (-1)\mathbf{P}_i(\mathbf{D}_\perp \cdot \mathbf{D}_\perp^*) + \mathbf{D}_\perp(\mathbf{P}_i \cdot \mathbf{D}_\perp^*) + \mathbf{D}_\perp^*(\mathbf{P}_i \cdot \mathbf{D}_\perp) \\ & + \mathbf{D}_\perp N^* + \mathbf{D}_\perp^* N + i(\mathbf{D}_\perp N^* - \mathbf{D}_\perp^* N) \times \mathbf{P}_i + i\mathbf{D}_\perp \times \mathbf{D}_\perp^*, \end{aligned} \tag{5}$$

where P_f is the polarisation vector of the scattered neutrons. On the one hand, Eq. (5) shows that pure nuclear scattering ($\mathbf{D}_\perp = 0$) leaves the polarisation of the neutron beam unchanged. On the other hand, polarisation of the scattered beam is obtained either, as we will see in the next section, by scattering neutrons on mixed nuclear–magnetic Bragg reflections or from a helicoidal magnetic structure. In the latter case, with $\mathbf{D}_\perp N^* + \mathbf{D}_\perp^* N = 0$, a polarised beam with a polarisation given by

$$P_f = \frac{i\mathbf{D}_\perp \times \mathbf{D}_\perp^*}{\sigma} = \frac{i\mathbf{D}_\perp \times \mathbf{D}_\perp^*}{\mathbf{D}_\perp \cdot \mathbf{D}_\perp^*} \qquad (6)$$

is created. We point out that a measurement of the chiral term provides the helicity of a helicoidal magnetic structure as has been shown by Shirane *et al.* (1983). In the general case, the polarisation vector of the neutron beam after scattering is rotated with respect to P_i and its length is not necessarily equal to $|P_i|$. The term "*polarisation analysis*" therefore refers to the determination of the direction and length of P_f.

§ 3. Production of Polarised Neutrons

For a measurement of the polarisation dependence of cross sections various techniques for producing and analysing polarised neutron beams have been developed. Depending on the required phase space properties of the beams, i.e., continuous vs pulsed, energy, divergence, type of detector, etc., different methods for the spin analysis are used. The most common methods are diffraction from single-crystal polarisers (mostly Heusler), reflection from magnetised thin film multilayers or supermirrors and absorption of the nonwanted spin state by means of polarised ^{3}He. A recent review of these techniques can be found in Anderson *et al.* (2000).

Single-Crystal Polarisers

This method produces a polarised neutron beam by taking advantage of the magnetic–nuclear interference term in Eq. (4) and Eq. (5). If a magnetic field is applied to a centrosymmetric crystal so that all the magnetic moments are saturated and aligned perpendicular to the scattering vector $\mathbf{Q}$, the neutron scattering cross section for Bragg scattering is given by (set $P_i = 0$ and $\mathbf{D}_\perp = \mathbf{D}_\perp^*$ in Eq. (4))

$$\sigma = N^2 + D_\perp^2. \qquad (7)$$

The second master equation, Eq. (5), yields for $P_i = 0$

$$P_f = \frac{2N\mathbf{D}_\perp}{\sigma} = \frac{2N\mathbf{D}_\perp}{N^2 + D_\perp^2}. \qquad (8)$$

Hence, the diffracted beam from a single crystal is completely polarised if there is a Bragg reflection with $|\mathbf{D}_\perp| = |N|$. Typical examples are the (111) reflection of Heusler Cu_2MnAl (d spacing = 3.43 Å) and the (200) reflection of the alloy $Co_{0.92}Fe_{0.08}$ (d spacing = 1.76 Å). Other single crystals like Fe_3O_4 or Fe_3Si have also been considered but are less used. All these crystals can be used to produce polarised and monochromatic neutron beams and to analyse the energy and polarisation of neutron beams. Therefore, single-crystal polarisers are used for single-crystal diffractometers and in triple-axis spectroscopy. Depending on the requirements for neutron energy and resolution, different d spacings must be considered. Recently, the quality and the reflectivity of Heusler monochromators have been improved considerably (Courtois, 1999) which will make it possible to use these crystals at relatively short neutron wavelengths.

Thin Films

Total reflection from magnetised thin films can be used to produce polarised neutrons. The angle of total reflection for a ferromagnetic film is given by

$$\theta_c^{\pm} = \lambda\sqrt{N(b \pm p)/\pi}, \qquad (9)$$

where λ is the neutron wavelength, N is the nuclear density and b and p are the nuclear and magnetic scattering lengths, respectively. Thus, by an appropriate choice of materials, a polarised beam can be produced by total reflection. For the special case $b = p$ all reflected neutrons are polarised. Unfortunately, the reflection angles are only reasonably large for cold neutrons: For example, $Fe_{50}Co_{48}V_2$ has $b \simeq p$ and $\theta_c \simeq 0.4°$ for $\lambda \simeq 4$ Å (Schärpf, 1975).

The angles of reflection can be significantly improved by adding artificial magnetic and nonmagnetic layers that reflect neutrons at small angles above θ_c. Such artificial multilayers (supermirrors) were produced for the first time by physical vapor deposition by Mezei (Mezei, 1976; Mezei and Dagleish, 1977). Typical material combinations are Co/Ti, Fe/Si, and $Fe_{50}Co_{48}V_2/TiNi_x$ (Hoghoj *et al.*, 1999; Krist *et al.*, 1999; Lee and Majkrzak, 1999; Syromyatnikov *et al.*, 1999; Anderson *et al.*, 2000). The latter combination exhibits a remanent magnetisation and can therefore be used as a spin selective device, where no spin flipper is necessary anymore (Böni, 1996; Böni *et al.*, 1999). Recently, the number of layers has been increased steadily, thus leading to reflection angles for polarised neutrons on the order of 0.3° for $\lambda \simeq 1$ Å. These modern devices can now also be used as white beam polarisers for thermal neutrons.

Spin Filters

A major drawback of polarising single crystals and thin films is their decreasing efficiency with

increasing neutron energy, i.e., short wavelength, and the small divergence that they accept (see Table 1). On the other hand they are maintenance free and easy to use. Therefore, polarising filters with broadband characteristics and minor restrictions on divergence are of significant interest for neutron scattering in particular for pulsed spallation sources and spectrometers with large area detectors.

Whereas Heusler and supermirrors are well established but still progressing techniques, the ^{3}He spin filters using direct optical pumping of metastable ^{3}He (Colgrove *et al.*, 1963) have improved during the past few years (Heil *et al.*, 1999). The basic idea behind the filter technique is the polarisation dependence of the transmission that can be written in its most simple form as (Williams, 1988)

$$T(\lambda) = \exp(-\sigma_0 N d)\cosh(\sigma_p N d), \qquad (10)$$

where λ is the neutron wavelength, d the thickness of the filter and N the ^{3}He density. σ_0 and σ_p are the spin-independent and polarisation-dependent cross sections of ^{3}He, respectively. If the filter is not perfectly polarised, a significant portion of the correctly polarised neutrons will be absorbed. Because the absorption increases with increasing λ, the thickness d of the filter must be optimised for the wavelength band to be used even if σ_0 is small.

^{3}He filters are now in regular use at the ILL on several instruments. Due to wall relaxation of polarised He nuclei, the polarisation and transmission of the filters decreases with time and they must be exchanged. It is foreseen that ^{3}He filters will further improve and find applications in particular at pulsed neutron sources and instruments with large area detectors. The method of using spin exchange of ^{3}He with optically pumped Rb vapor (Bouchiat *et al.*, 1960) is progressing too and may challenge the metastable type of pumping. One major advantage of the latter technique is that the filter does not have to be exchanged during an experiment.

The development of $SmCo_5$ polarising filters has been conducted at ISIS. If the problems of depolarisation of the neutrons within the filter and of γ-heating in intense neutron beams can be solved one may obtain a quality factor of $Q \simeq 0.25$ (Mayers *et al.*, 1986) that is lower than the maximum to be achieved for a future ^{3}He filter.

Polarised hydrogen can also be used as a polarising filter. Moreover, the spin-dependent interaction of the neutrons with the protons can be used for contrast variation of hydrogen-containing materials in small-angle neutron scattering experiments (Stuhrmann, 1999). We defer the interested reader to the literature.

§4. Determination of Form Factors and Spin Densities

Polarised neutrons make it possible to measure magnetic densities with improved accuracy as compared to that of standard diffraction methods. The method presented below applies to magnetic structures described by a propagation vector $\mathbf{Q}_0 = 0$. For a paramagnet, a ferromagnetic component can be induced by applying an external magnetic field. According to Eq. (4) in the case of mixed nuclear–magnetic Bragg reflections with real structure factors, the intensity ratio R of scattered neutrons polarised by an external magnetic field along the $+z$ or $-z$ direction, where z is perpendicular to the scattering plane (that contains Q), is given by

$$R = \frac{I^{+z}}{I^{-z}} = \frac{N^2 + 2ND_\perp^z + D_\perp^{z2}}{N^2 - 2ND_\perp^z + D_\perp^{z2}} = \frac{(N + D_\perp^z)^2}{(N - D_\perp^z)^2}. \qquad (11)$$

$D_\perp^z$ is the projection of the magnetic interaction vector $\mathbf{D}_\perp$ along the z axis. Determination of a spin density with polarised neutrons consists of measuring R at many different Bragg reflections (hkl). As the crystal structure and hence the chemical structure factors N are presumably known (N depends on the Miller indices), the method provides usually directly the values of the magnetic structure factors. For small magnetic amplitudes, polarised neutrons give an enhanced sensitivity compared to unpolarised neutrons that yield an intensity $I_{np} = N^2 + \frac{2}{3}D_\perp^2$. The factor 2/3 comes from the spherical averaging of $\mathbf{D}_\perp$ in the second term

Table 1 Performance and Applications of Various Neutron Polarisers.

Technique	*Beam*	*E range (meV)*	*Instruments*	*T*	*P*	*Q*	*Ref.*
Heusler	fixed λ	$E < 80$	TAS, DAX	0.62	0.95	0.56	Courtois (1999)
Supermirror	white	$E < 20$	NSE, TAS, REF, TOF	0.9	0.95	0.81	Hoghoj *et al.* (1999)
^{3}He	white	$E < 2000$	DAX, TAS, TOF, SANS	0.4	0.80	0.26	Heil *et al.* (1999)
p targets	white	$E \gg 2000$	SANS	0.4	0.80	0.26	Heil *et al.* (1999)
$SmCo_5$	white	$20 < E < 180$	Not implemented	0.3	0.75	0.17	Mayers *et al.* (1986)

Note. The quoted values are only approximate. The notation is TAS, triple-axis spectrometer; DAX, double-axis diffractometer; NSE, neutron spin echo; REF, reflectometer; TOF, time of flight; and SANS, small-angle neutron scattering. The quality factor is defined by $Q = TP^2$, where the transmission/reflection T and polarisation P are taken from the literature.

of Eq. (4) over all directions with respect to Q for a nonmagnetised isotropic sample.

Namely, considering a typical example with $D_\perp = 0.1N$ yields $I_{np} \simeq 1.01N^2$, while the contrast as measured with polarised neutrons, $R = 1.21N^2/0.81N^2 = 1.49$, is rather large. Therefore polarised neutrons are particularly well suited for measuring maps in compounds with small magnetic moments (for example, heavy fermion systems) or with seriously diluted magnetic moments (for example, molecular magnetic crystals).

To extract the magnetic moment density from the data, a classical Fourier calculation is usually performed (for a recent review, see Schweizer (1995)). Because

$$\rho(\mathbf{Q}) = \int\int\int m(\mathbf{r}) \exp(i\mathbf{Q}\cdot\mathbf{r}) d^3\mathbf{r}, \qquad (12)$$

one can obtain the spin density $m(\mathbf{r})$ in real space by the inverse Fourier transform through the relation

$$m(\mathbf{r}) = \frac{1}{V}\sum_{\mathbf{Q}} \rho(\mathbf{Q}) \exp(-i\mathbf{Q}\cdot\mathbf{r}). \qquad (13)$$

As the cloud of unpaired electrons that are responsible for magnetism is extended in real space, the magnetic **form factor** decreases with increasing Q and equivalently with increasing Bragg indices (hkl). To obtain precise measurements, data are to be taken up to large values of scattering vectors Q. To that end short-wavelength neutrons are to be preferred, and instruments dedicated to such measurements provide usually hot neutrons, like the double-axis diffractometers D3 at the ILL and 5C1 at the LLB. The layout of such an instrument is presented in Fig. 1. Until now, no polarised neutron diffractometers have been built at a spallation source. In any case, however, the data set is restricted to finite values of h, k, l, which leads to oscillatory distortions in the spin density maps $m(\mathbf{r})$ due to finite size effects (Schweizer, 1995). Therefore, other reconstruction methods of the spin density map have been developed. The two most often used techniques are based either on information theory like the maximum entropy method (Papoular and Gillon, 1990a,b) or on the multipolar expansion of the electronic density (Gillon and Schweizer, 1989). The latter method models the spin density by a set of parameters that must be determined by standard least-squares fitting calculations.

Figure 1 Schematic arrangement of a two-axis spectrometer used for the determination of magnetic densities. The monochromator produces a polarised beam with the neutron polarisation perpendicular to the scattering plane. A small guide field prevents the neutron beam from depolarising. A *spin flipper* makes it possible to reverse the neutron polarisation by 180° and hence to measure the flipping ratio R. A magnetic field saturates the magnetic moments of the sample along the neutron polarisation.

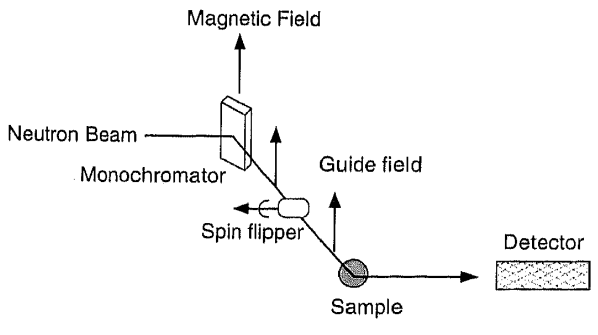

Magnetic Form Factors

Ever since the experiments of Shull and co-workers in the 1960s on 3d ferromagnets (Shull and Yamada, 1962; Moon, 1964; Mook, 1966), the main motivation to measure spin densities has been to gain a better insight into electronic distributions in solid-state materials. Since that time, measurements have been extended to paramagnetic metals and to the 4*f*-electrons in rare-earth compounds (Boucherle *et al.*, 1982; Moon, 1982, and references therein).

Whereas in 3d ferromagnets the atomic form factor can be very precisely reproduced from spin-polarised Hartree–Fock calculations (Watson and Freeman, 1961), there is a strong indication from form factor measurements of a negative spin polarisation between the atomic sites in both Fe and Co. Also, the magnetic moment density map in Ni (Mook, 1966) and Pd (Cable *et al.*, 1975) shows an aspherical *d*-electron distribution plus an orbital contribution. In order to allow for these effects, the form factor is usually written as

$$f(\mathbf{Q}) = \frac{2}{g}(1+\alpha)\left[\langle j_0\rangle + (\frac{5}{2}\gamma - 1)A_{hkl}\langle j_4\rangle\right] + \left[\frac{(g-2)}{g} f_{orb} - (\frac{2}{g})\alpha\delta(\mathbf{Q})\right], \qquad (14)$$

where g is the Landé factor, α is a parameter describing the fraction of negative spin polarisation, γ is the percentage of electrons in E_g orbitals, which takes into account the orbital contribution (Mook, 1966). A_{hkl} is a geometrical factor and $\langle j_0\rangle$ and $\langle j_4\rangle$ represent the spherical and aspherical part of the form factor, respectively. A comparison of the calculated and measured form factors for Ni yielding a uniform negative contribution equal to $-0.0091\mu_B/\text{Å}^3$ is shown in Fig. 2. The spin magnetic moment per Ni atom is $\mu_{spin} = 0.656\mu_B$ and the orbital contribution $\mu_{orbital} = 0.055\mu_B$.

In contrast to metallic compounds with *d* electrons, *f* electrons are well localised around the nuclei, which makes it possible to perform atomic calculations to obtain the spin distribution. As the orbital moment is usually different from 0, there is a significant contribution of the orbitals to the magnetic density. Also, the spin–orbit coupling, which results in a mixing of

Figure 2 Magnetic moment distribution of Ni in the [100] plane (taken from Mook (1966)).

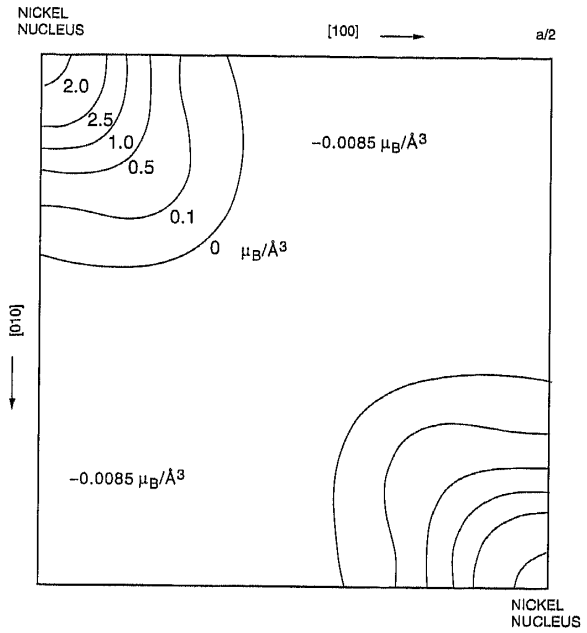

the atomic wave functions, is important. The form factors for the atoms of the rare-earth and actinide series have been calculated by Freeman and Desclaux (1979) using the relativistic Dirac–Fock theory. It was shown that the atomic form factor can be expressed as

$$f(\mathbf{Q}) = \langle j_0 \rangle + c_2\langle j_2 \rangle + c_4\langle j_4 \rangle + c_6\langle j_6 \rangle, \qquad (15)$$

where

$$\langle j_l(\mathbf{Q}) \rangle = \int_0^\infty U^2(r) j_l(Qr) 4\pi^2 dr. \qquad (16)$$

$U(r)$ is the radial wave function for the unpaired electrons in the atom, and $j_l(Qr)$ the Bessel function of lth order. The coefficients c_i are tabulated in, e.g., Brown (1992).

Among the rare-earth elements, Samarium represents a particular case as the orbital and spin contributions to the magnetisation almost cancel out so that the magnetic density map contains both positive and negative regions. This leads to a form factor that has a maximum located at a position different from $Q = 0$. The Sm form factor measured in $SmCo_5$ is shown in Fig. 3. An interesting effect is that as the first excited crystal-field states are located at relative low energies, they become populated when the temperature approaches 300 K. Consequently, the magnetic moment of Sm is only $\mu \sim 0.04\mu_B$ at room temperature and increases to $\mu \sim 0.38\mu_B$ for $T = 4.2$ K (Givord *et al.*, 1979). For all temperatures, however, the form factor of Sm has a strong orbital character.

Finally, we should point out that a study of the spatial distribution and temperature dependence of the spin density makes it possible to probe the spin susceptibility $\chi(\mathbf{Q}, 0)$. As such the method can be

Figure 3 (a) Experimental form factor for Sm at $T = 4.2$ K. The line corresponds to a calculation including crystal field, exchange and spin–orbit effects. (b) Same for $T = 300$ K (taken from Givord *et al.* (1979)).

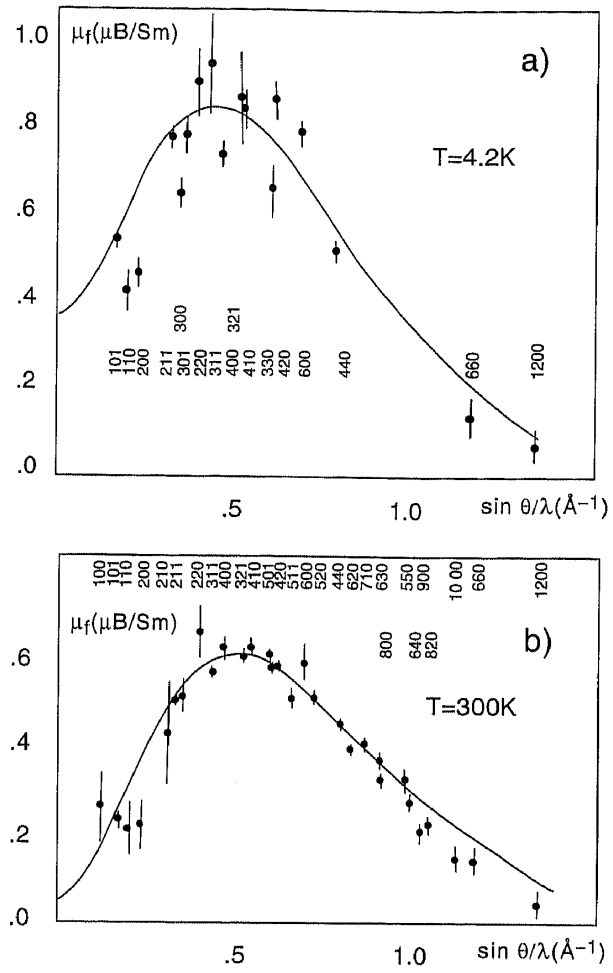

used to investigate the nature of the electrons, e.g., in superconductors. For example, in V_3Si (Shull and Wedgwood, 1966), it was shown that the spin susceptibility of the V electrons disappears upon entering the superconducting phase, which is an indication of spin pairing. On the other hand, no similar effect could be observed in the new heavy-fermion superconductors UPt_3, UBe_{13} and $CeCu_2Si_2$. For the latter compounds, the spin susceptibility is temperature independent in the superconducting phase (Stassis *et al.*, 1986). These results are of particular importance as they impose severe restrictions on the possible pairing mechanisms that can give rise to the electron pairing in these unconventional heavy-fermion superconductors.

Magnetisation Distribution in Molecular Magnets

Molecular magnetism is a fast growing field in material science with potential important technological applications in electronic devices. By building blocks of molecules that contain magnetic centres, magnetic interactions can be tuned and the aim is to synthesize organic compounds that exhibit magnetic ordering at

room temperature. To that end, as the number of combinations offered by organic chemistry is almost infinite, it is essential for the mechanism of magnetic couplings originating from $2p$ electrons to be well understood (Kahn, 1993).

In contrast to ionic systems where the electrons that carry magnetism are well localised around the nuclei, the magnetic density of organic compounds is distributed over all molecules due to covalency effects. The effect of delocalisation is even more pronounced when there is no magnetic ion in the molecule and magnetism is due to $2p$ electrons only (Schweizer, 1997). Polarised neutron diffraction yields directly the distribution of electrons responsible for magnetism in organic materials, which in turn can be directly compared to theoretical calculations for the electronic wave functions and the chemical bonds (Ressouche, 1999). Spin density in molecular compounds can also be used to trace exchange pathways through the molecules, like when spin polarisation is found on atoms that in principle are nonmagnetic. This is for example the case in the free radical nitronyl nitroxides NitPy(C≡C–H). NitPy(C≡C–H) builds zig-zag chains linked by C≡C–H···O pieces where the hydrogen bridge two molecules. As shown in Fig. 4, significant spin population is found at the hydrogen positions ($\mu \sim 0.04\mu_B$), which indicates that the hydrogen bond is involved in the ferromagnetic exchange interactions between the molecules (Pontillon *et al.*, 1997).

A typical example of *spin delocalisation* is found in the compound $MnCu(pba)(H_2O)_3 \cdot 2H_2O$, with pba=1,3-propylenebis(oxamato). The Mn^{2+} and Cu^{2+} ions are connected by oxamato bridges and build ferrimagnetic chains. The Mn^{2+} ions carry a spin $S_{Mn} = \frac{5}{2}$ and the Cu^{2+} have an effective spin $S_{Cu} = \frac{1}{2}$. Therefore we have the situation where two magnetic metals are linked by organic species. The magnetisation, as obtained from polarised neutron diffraction (Baron *et al.*, 1993, 1996), shows a positive spin population (i.e., the induced magnetisation is aligned along the applied magnetic field) for the Mn spins, whereas it is negative for the copper magnetic moments. This reveals the antiferromagnetic nature of the intrachain coupling. Interestingly, an important contribution to the spin density map is found on the neighbouring oxygen and nitrogen ions and on the two central carbon atoms. Summing up the positive and negative spin polarisations individually, one obtains $5.1\mu_B$ and $-1.0\mu_B$, respectively, which shows that the metallic ions have distributed their spin densities on the molecule. The magnetic moment distribution for $MnCu(pba)(H_2O)_3 \cdot 2H_2O$ is shown in Fig. 5.

Figure 5 also shows the theoretical spin density for the "CuMn" molecule projected onto the oxamid mean plane. The theory is based on the local

Figure 4 Spin density projection in NitPy(C≡C–H). The contour step for the pyridine cycle is $0.008\mu_B/Å^2$, whereas for the Nit cycle a step is equal to $0.04\mu_B/Å^2$ (taken from Pontillon *et al.* (1997)).

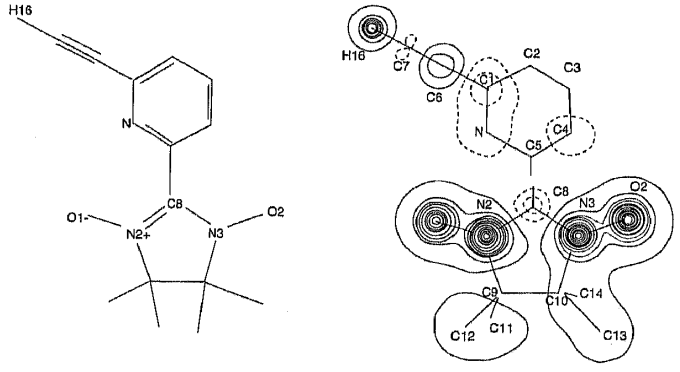

Figure 5 (a) Experimental spin-density map of MnCu(pba)$(H_2O)_3 \cdot 2H_2O$. The contour step is $0.005\mu_B/Å^2$. The continuous line represents the positive spin distribution while the dotted line describes the negative magnetisation. (b) Calculated spin density map for an isolated molecule with the DMol^3 method (after Baron *et al.* (1996)). The lowest contour is at $0.005\mu_B/Å^2$.

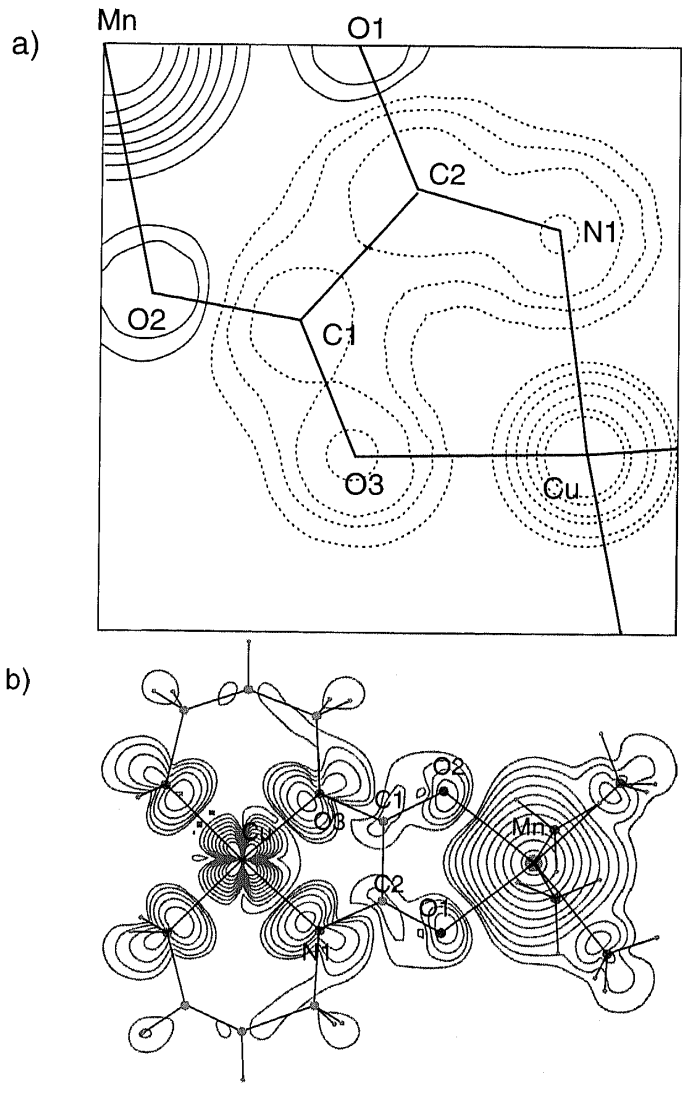

spin-density functional principles of Perdew and Wang (1992). Calculations for the cation (2+) in vacuum are done with the DMol[3] method (Delley, 1990, 2000). On comparing with experiment it is clear that there is a disagreement with theory on the sign of the spin density at the bridging carbon atoms. One should remember, however, that the theory applies to an isolated cation in vacuum. Calculations for smaller than the formal charge reverse the spin density at the bridging carbons. The crystal environment may also change areas with small spin density.

Spin Susceptibility in the High-T_c Superconductor $YBa_2Cu_3O_{7-x}$

The discovery of the high-T_c superconductor $La_{2-x}Ba_xCuO_4$ with $T_c = 35$ K by Bednorz and Müller (1986) has been at the origin of an enormous amount of work to understand the electronic (charge and spin) correlations in these materials. Following the discovery of the $La_{2-x}Ba_xCuO_4$ compound, other materials exhibiting similar or higher transition temperatures for superconductivity have been synthesised, like $La_{2-x}Sr_xCuO_4$, $Nd_{2-x}Ce_xCuO_4$, $YBa_2Cu_3O_{7-x}$ and others. All these materials share common features of their crystallographic structure. They possess CuO_2 layers well separated from each other, so that they can be considered as quasi-two-dimensional materials. In this class of materials, superconductivity is achieved by carefully tuning the amount x of Sr, Ce or O, which results in doping the CuO_2 layers with charge carriers. The important feature is that the cuprate materials are *either* antiferromagnets and insulators *or* paramagnetic metals and superconductors below a critical temperature T_c. Important antiferromagnetic correlations and fluctuations persist in the superconducting phase. The role played by these fluctuations in the formation of the superconducting state is still the subject of an intense debate. A central piece of the physics of the high-T_c superconductors is the understanding of the charge and spin states in the CuO_2 layers as a function of doping both below and above the transition temperature T_c.

The intensity of the scattered neutrons can be directly related to the spin susceptibility at $\mathbf{Q} = 0$ and $\omega = 0$ through the dissipation–fluctuation theorem. As the signal is particularly small in the high-T_c compounds, use of polarisation analysis is required to enhance the contrast and to isolate the weak magnetic contribution. The results obtained for the temperature variation of the local susceptibility at the copper sites in the CuO_2 layers is shown in Fig. 6. A particularity of the temperature dependence of the signal is the appearance of the so-called *spin pseudo-gap* in underdoped $YBa_2CuO_{6.52}$ for which

Figure 6 Local spin susceptibility as a function of temperature on copper sites in the CuO_2 layers in the high-T_c superconductors $YBa_2Cu_3O_{7-x}$ (taken from Regnault *et al.* (1998)).

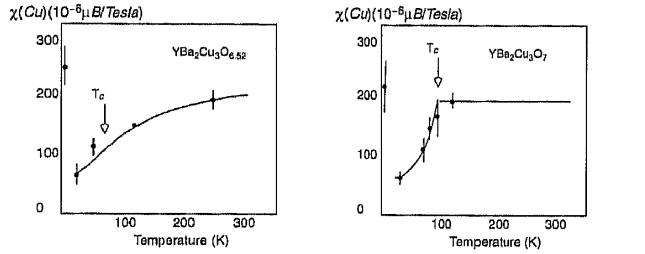

the spin susceptibility drops above T_c. On the other hand, the local spin susceptibility in optimal doped samples decreases only upon cooling below the superconducting temperature (Boucherle *et al.*, 1993; Henry *et al.*, 1994).

§5. Spherical Neutron Polarimetry

Spherical neutron polarimetry (SNP) has recently been developed and successfully tested at the ILL (Brown *et al.*, 1993) as an alternative way of measuring magnetic structures. Moreover, this method makes it possible to determine form factors and spin densities in antiferromagnets for which very few data are available. The classical technique discussed in §4 cannot be applied in antiferromagnets with propagation vector $\mathbf{Q}_0 = 0$ when the magnetic and nuclear structure factors are in phase quadrature. For such cases, like Cr_2O_3 or even hematite, the neutron cross section σ is polarisation independent (Brown *et al.*, 1999) when using that

$$\mathbf{P}_f\sigma = \mathbf{P}_0(1-\gamma^2) + 2\gamma^2\hat{\mathbf{Q}}(\mathbf{P}_0\cdot\hat{\mathbf{Q}}) + 2\gamma(\mathbf{P}_0\times\hat{\mathbf{Q}}), \qquad (17)$$

with $\sigma = 1+\gamma^2$ and $\gamma\hat{\mathbf{Q}} = \Im\mathbf{D}_\perp(\mathbf{Q})/N$. On the other hand SNP gives access to the complete set of independent correlation functions involved in the nuclear–magnetic scattering process by a direct measurement of the three components of the polarisation vector $\mathbf{P}_f$ of the scattered neutrons. Equation (5) shows that if the polarisation $\mathbf{P}_i$ of the incoming neutron beam is fixed, a measurement of $\mathbf{P}_f$ allows in most cases an unambiguous determination of the direction of the magnetic interaction vector $\mathbf{D}_\perp$. This is an alternative way of determining magnetic structure factors to the standard diffraction method that relies on a precise measurement of neutron intensities. Measuring intensities with unpolarised neutrons is the same as measuring $\mathbf{D}_\perp\cdot\mathbf{D}_\perp^*$, which leads to a loss of phase factors and often magnetic structures cannot be unambiguously resolved by diffraction. SNP has been successfully applied in problems involving complex magnetic structures, like spiral structures, systems with magnetic domains and small magnetic moments, and frustrated antiferromagnets. It must be pointed out that the method is sensitive to the direction of the magnetic

interaction vector only and not to its magnitude. In this case, finding the value of magnetic moments requires, as usual, the comparison of magnetic and nuclear cross sections. In contrast to standard single-crystal diffraction, it is insensitive to secondary extinction and allows magnetic structure determination of samples even in the presence of magnetic domains. Namely, magnetic domains depolarise the neutron beam according to their respective population. In other words, the domain population is obtained by measuring the amplitude of the neutron polarisation vector $\mathbf{P}_f$. In order to perform spherical neutron polarimetry a nonisotropic domain distribution is usually necessary. It can be induced for example by the application of uniaxial pressure.

Spherical neutron polarimetry outperforms standard polarised neutron scattering as it makes it possible to measure both the longitudinal and transverse components of $\mathbf{P}_f$. Namely, if a magnetic field is applied to the sample, as is the case for the longitudinal polarimetry explained in §4, only the component of the polarisation longitudinal to the field can be measured. The transverse components depolarise rapidly and are lost (Newton and Kittel, 1948). This is the case in antiferromagnets with mixed nuclear–magnetic Bragg reflections, where most information is contained in the transverse components through the nuclear–magnetic interference term.

Realisation of a Zero-Field Chamber: Cryopad

Following the introduction in the previous section it is clear that the transverse components of the polarisation can only be measured if the sample is placed in a zero-field chamber. Such a device (called Cryopad) has been constructed at the ILL (Fig. 7) (Tasset *et al.*, 1999). It consists of two cylindric Meissner shields in the superconducting state. The diameter of the inner shield is large enough to accommodate a cryostat and/or other devices to define the sample environment. Cryopad is centred on the sample table and its orientation is fixed with respect to the wave vector $\mathbf{k}_i$ of the incident neutrons. Therefore, the sample can be oriented independently from Cryopad in order to access various Bragg reflections.

Figure 7 Schematic zero-field chamber *Cryopad II* used for spherical polarimetry at ILL (taken from Tasset *et al.* (1999)).

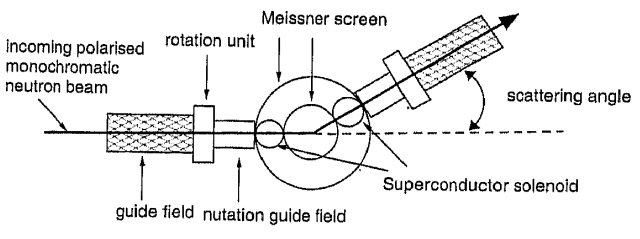

The components of the polarisation of the incident and scattered neutrons are defined independently by means of two rotating solenoids (called *nutators*) that are placed in the incident and scattered neutron beam. They act as guide fields in order to orient the neutron polarisation vectors $\mathbf{P}_\alpha$ (α = incident, final) in the plane parallel to the Meissner shields (transverse to $\mathbf{k}_\alpha$). Two spin-turning coils between the Meissner shields apply a horizontal field transverse to $\mathbf{k}_\alpha$ and allow the definition of the component of $\mathbf{P}_\alpha$ along $\mathbf{k}_\alpha$. The modulus of $\mathbf{P}_f$ is determined by measuring the flipping ratio of the scattered neutrons simply by reversing the field of the nutator after the sample. This can be accomplished quickly by reversing the current in the solenoid. The combined use of the nutators and of the spin-turning coils in Cryopad allows the analysis of $\mathbf{P}_f$ for any direction of $\mathbf{P}_i$. In practice, the information is obtained by measuring the three orthogonal components of the final polarisation P_f^α ($\alpha = x, y, z$) for the three orthogonal directions of the initial polarisation $\mathbf{P}_i$. The direction x is defined as being along the scattering vector $\mathbf{Q}$, z is chosen perpendicular to the scattering plane and y is the last orthogonal direction. For example, if the initial polarisation is chosen along the z axis, the component of the final polarisation along the x direction is given by $P_x = (n_{x+} - n_{x-})/(n_{x+} + n_{x-})$, where n_{x+} and n_{x-} are the number of neutrons with spins along or antiparallel to the x axis, respectively (Tasset *et al.*, 1999). Measuring the nine flipping ratios is sufficient for determining the required information about the orientation of the magnetic interaction vector $\mathbf{D}_\perp(\mathbf{Q})$ and to obtain the value of the ratio between magnetic and nuclear amplitudes $|\mathbf{D}_\perp(\mathbf{Q})|/N$. Geometrical relationships between the direction of the final neutron polarisation relative to $\mathbf{P}_i$ have been derived by Nunez *et al.* (1991) and are of great help to determine the direction of $\mathbf{D}_\perp(\mathbf{Q})$.

Example: UPtGe

Heavy-fermion materials are characterised by a very large linear coefficient of the specific heat and a greatly enhanced Pauli susceptibility, corresponding to effective masses of the quasi-particles of about two orders of magnitude larger than the free electron. Heavy fermions are therefore ideal systems for studying strong electron correlations and the number of compounds showing heavy-fermion behaviour is large. The ground state of these systems varies from metallic ($CeCu_6$, $CeIn_3$) to insulating ($Ce_3Bi_4Pt_3$) and from antiferromagnetic (U_2Zn_{17}, UPd_2Al_3, UNi_2Al_3) to superconducting (UPt_3, UPd_2Al_3, UNi_2Al_3, $CeCu_2Si_2$). In most of these systems the magnetic ground state is determined by the competition between the Kondo effect that tries

to screen the magnetic moment and the RKKY interaction that tends to stabilise a ground state with long-range magnetic order.

Noncollinear magnetic structures in compounds with localised spin densities can be explained on the basis of the Heisenberg model to originate from competition between exchange forces. In systems with *5f* electrons, like U_3P_4 or U_2Pd_2Sn, it has been shown by calculations based on the local spin-density functional theory that a noncollinear arrangement of the magnetic moments is the consequence of strong spin–orbit coupling (Sandratskii and Kübler, 1995). However, this theory does not favour the helicoidal type of magnetic structures found in UPtGe.

As an example of a magnetic structure determination with the help of spherical neutron polarimetry we show results obtained from the ternary compound UPtGe that orders below $T_N \sim 50$ K with a propagation vector $Q_0 = (0.554, 0, 0)$ (Robinson *et al.*, 1993). Measurements in single crystals using unpolarised neutrons could not decide between an amplitude-modulated spin-density wave and a cycloid with unequal magnetic moments along the *a* and *c* axes (ellipticity), respectively, yielding for the two models similar agreement factors between observed and calculated structure factors (Szytula *et al.*, 1992; Robinson *et al.*, 1993).

It is seen from Eq. (5) that the direction and the amplitude of the polarisation of the scattered neutrons depend upon the value of the chiral term. In particular, the chiral component disappears, when $D_\perp(Q_0)$ is parallel to $D_\perp^*(Q_0)$, as is the case for an amplitude-modulated wave and the polarisation of the neutron precesses by 180° around the scattering vector (Nunez *et al.*, 1991). In contrast, the chiral term gives a contribution to P_f if the magnetic structure is a cycloid. Hence, the direction of P_f depends on the scattering geometry. Spherical neutron polarimetry therefore makes it possible to distinguish between an amplitude-modulated spin-density wave and a helix (Paixão *et al.*, 2000). For UPtGe, the directions of polarisation of the diffracted neutrons for directions of P_i perpendicular to the scattering plane (z), along the scattering vector (x), and along a third direction in the scattering plane but perpendicular to x are summarised in Table 2. The results of spherical neutron polarimetry unambiguously show that the magnetic structure of UPtGe is a cycloid with an axis ratio ~1.24 (Mannix *et al.*, 2000) as shown in Fig. 8.

§ 6. Inelastic Neutron Scattering with Polarised Neutrons

In analogy to the neutron cross section derived by Blume (1963) for the elastic case, there are three contributions to the inelastic cross section:

- a pure nuclear one that gives rise to phonon scattering,
- a pure magnetic one when neutrons are scattered, e.g., by spin waves and
- a magnetic–nuclear interference term that is present only in special cases, as, e.g., when the spin–lattice interaction in a ferromagnet cannot be neglected.

The inelastic neutron cross section and its relationship to the neutron polarisation have been derived by many authors (see, e.g., Squires (1978) and

Table 2 Spherical Neutron Polarimetry Data Obtained with Cryopad in UPtGe (after Mannix *et al.* (2000)).

	P_i			P_f			P_{calc}		
hkl	*x*	*y*	*z*	*x*	*y*	*z*	*x*	*y*	*z*
0^+00	0	0	0.9	0.01	−0.05	0.91	0	0	0.90
	0	0.9	0	0.08	−0.91	−0.04	0	−0.90	0
0^+20	0	0	0.9	0.94	−0.11	−0.12	0.97	0	−0.11
	0	0.9	0	0.94	−0.02	0.03	0.97	0.11	0
2^-20	0	0	0.9	−0.91	0	0.16	−0.95	0	0.20
	0	0.9	0	−0.91	−0.10	−0.01	−0.95	−0.2	0
0^-20	0	0	0.9	−0.93	0.05	−0.14	−0.97	0	−0.11
	0	0.9	0	−0.92	0.13	−0.02	−0.97	0.11	0
	0	0	−0.9	−0.92	0.14	0.09	−0.97	0	0.11
	0	−0.9	0	−0.93	0	−0.04	−0.97	−0.11	0

Note. P_i, P_f and P_{calc} are the incident, scattered and calculated neutron polarisations. The polarisation axes are defined as *x* being parallel to the scattering vector **Q**, *y* being perpendicular to **Q** and in the scattering plane and *z* being vertical.

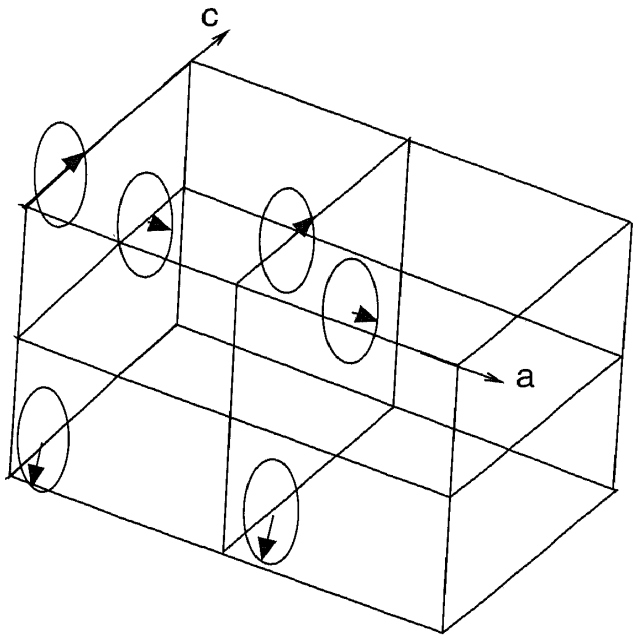

Figure 8 Magnetic structure of UPtGe as determined by spherical neutron polarimetry using the Cryopad device (after Mannix *et al.* (2000)).

Lovesey (1984)). In the following we shall reproduce the calculations of Maleyev (1999), which expresses the time-dependent scattering amplitudes in terms of the Van Hove correlation function

$$\pi S_{AB}(\omega) = \frac{1}{1-\exp(-\omega/T)} < A, B >''_{\omega}, \qquad (18)$$

where $< A, B >''_{\omega}$ is the absorptive part of the generalised retarded susceptibility

$$< A, B >''_{\omega} = \pi(1-\exp(-\omega/T))Z^{-1}\sum_{a,b}\exp(-\frac{E_a}{T}) \times A_{ab}B_{ba}\delta(\omega+E_{ab}). \qquad (19)$$

A and B are operators like $N(\mathbf{Q})$ or $\mathbf{D}_{\perp}(\mathbf{Q})$ from Eq. (4); Z^{-1} is the partition function and $E_{a,b}$ are the energies between eigenstates of the system. Expressed in such terms, the inelastic neutron cross section is given by

$$\sigma = \sigma_n + \sigma_m + \sigma_{nm}, \qquad (20)$$

with

$$\sigma_n = \frac{k_f}{k_i}\frac{1}{\pi}\frac{1}{1-\exp(-\omega/T)} < N(-\mathbf{Q}), N(\mathbf{Q}) >''_{\omega}$$

$$\sigma_m = \frac{k_f}{k_i}\frac{1}{\pi}\frac{1}{1-\exp(-\omega/T)} < D^{\alpha}_{\perp}(-\mathbf{Q}), D^{\beta}_{\perp}(\mathbf{Q}) >''_{\omega} \times(\delta_{\alpha\beta}+i\epsilon_{\alpha\beta\gamma}P_{i\gamma})$$

$$\sigma_{nm} = \frac{k_f}{k_i}\frac{1}{\pi}\frac{1}{1-\exp(-\omega/T)}(< N(-\mathbf{Q}), \mathbf{D}_{\perp}(\mathbf{Q}) >''_{\omega} + < \mathbf{D}_{\perp}(-\mathbf{Q}), N(\mathbf{Q}) >''_{\omega})\cdot \mathbf{P}_i. \qquad (21)$$

$\{\alpha, \beta, \gamma\} = \{x, y, z\}$ in Cartesian coordinates. The polarisation vector $\mathbf{P}_f$ is accordingly given

- for nuclear scattering by $\mathbf{P}_f\sigma_n = \mathbf{P}_i\sigma_n$,
- for pure magnetic scattering by

$$P_{f\alpha}\sigma_m \propto P_{i\beta}(< D^{\alpha}_{\perp}(-\mathbf{Q}), D^{\beta}_{\perp}(\mathbf{Q}) >''_{\omega} + < D^{\beta}_{\perp}(-\mathbf{Q}), D^{\alpha}_{\perp}(\mathbf{Q}) >''_{\omega}) - \delta_{\alpha\beta} < D^{\gamma}_{\perp}(-\mathbf{Q}), D^{\gamma}_{\perp}(\mathbf{Q}) >''_{\omega} - i\epsilon_{\alpha\beta\gamma} < D^{\beta}_{\perp}(-\mathbf{Q}), D^{\gamma}_{\perp}(\mathbf{Q}) >''_{\omega},$$

- for magnetic–nuclear interference scattering by

$$\mathbf{P}_f\sigma_{nm} \propto < N(-\mathbf{Q}), \mathbf{D}_{\perp}(\mathbf{Q}) >''_{\omega} + < \mathbf{D}_{\perp}(-\mathbf{Q}), N(\mathbf{Q}) >''_{\omega} + i[< N(-\mathbf{Q}), \mathbf{D}_{\perp}(\mathbf{Q}) >''_{\omega} - < \mathbf{D}_{\perp}(-\mathbf{Q}), N(\mathbf{Q}) >''_{\omega}] \times \mathbf{P}_i.$$

It turns out from these equations that, whereas phonons do not change the neutron polarisation, scattering by spin waves does. As we will see below this feature is very useful for separating and identifying the different magnetic modes in ferro- and antiferromagnets. For the particular cases of simple ferromagnets and of two-sublattice collinear antiferromagnets, explicit expressions for the polarisation dependence of the inelastic neutron cross section can be found in the classic paper of Izyumov and Maleev (1962). The magnetic–nuclear interference term gives rise in particular to the so-called *magneto-vibrational* scattering and is also important for a proper understanding of *magneto-elastic* scattering. Their origins are due to the fact that the cloud of electrons that carries magnetism follows the nuclei when they oscillate around their equilibrium position and that the magnetic moment is modulated by the lattice vibrations, respectively. The magneto-vibrational scattering is inelastic in the nuclear system but elastic in the magnetic one. It occurs at the same positions in reciprocal space as the phonons but with a polarisation dependence. It has been exploited, e.g., to measure the magnetic form factor through the polarisation dependence of phonons at general Q positions in Fe (Steinsvoll *et al.*, 1981).

Longitudinal Neutron Polarimetry

The first spectrometer that allowed the analysis of the scattered neutrons was built by Moon, Riste and Koehler by replacing the monochromator and analyser of a triple-axis spectrometer with ferromagnetic crystals that were saturated in a magnetic field (Fig. 9) (Moon *et al.*, 1969). In contrast to spherical neutron polarimetry the polarisation is maintained by means of guide fields throughout the instrument. As a consequence, only the component of the neutron polarisation parallel or anti-parallel to the field direction can be measured, whereas the transverse components depolarise and are lost. In exactly the same way as the magnetic–nuclear interference term cannot be measured by standard diffraction, the same effect happens for the inelastic counterpart. The magnetic–nuclear interference contribution leads to

Figure 9 Schematic arrangement of the three-axis spectrometer for polarised neutrons used by Moon *et al.* (1969), at Oak Ridge National Laboratory.

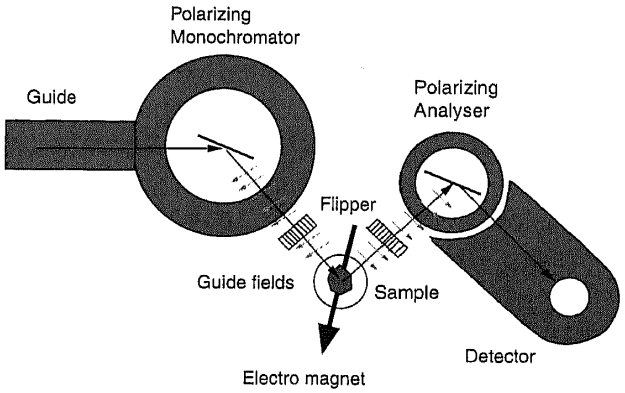

a rotation of the initial polarisation, which averages out if a magnetic field is applied. Such a contribution is only accessible if the sample is enclosed in a zero-field chamber, like the Cryopad device. The standard triple-axis instrument with polarisation analysis developed by Moon *et al.* makes it possible to measure the energy, momentum and spin dependence of cross sections with the restriction that only longitudinal polarimetry can be performed. In practice, two basic scattering geometries are commonly used: Namely the spin-flip and non-spin-flip cross sections are measured with the polarisation of the neutrons either parallel or perpendicular to the scattering vector Q.

An immediate application of longitudinal polarimetry is that for $P_i \parallel Q$ all magnetic scattering involves processes in which the spin of the neutrons is flipped because $D_{\perp z} = 0$. We point out again (see Eq. (3)) that this is a general rule valid for elastic and inelastic as well as coherent and incoherent scattering. In contrast, if the scattering geometry is chosen such that $P_i \perp Q$ and $M \parallel P_i$ then the elastic magnetic scattering ($D_x = D_y = 0$) is non-spin flip, whereas the inelastic scattering is spin flip (δD_y, transverse excitations) and non-spin flip (δD_z, longitudinal excitations), respectively.

Polarised neutrons in inelastic neutron scattering are often used to separate the magnetic from the nuclear scattering or to distinguish magnetic fluctuations perpendicular and transverse to the magnetisation or scattering vector. When scattering by phonons dominates a neutron spectrum an unambiguous determination of the magnetic contribution to the neutron cross section can be accomplished by measuring the scattering with $P_i \parallel Q$. A typical example for UFe_2 is shown in Fig. 10, where the linear dispersion curve of the acoustic phonons can be distinguished from the quadratic dispersion curve of the spin-wave branch in UFe_2 at low T in the crossover regime (Paolasini *et al.*, 1996).

Figure 10 Constant-energy inelastic scan in UFe_2 using polarisation analysis showing that spin waves occur in the spin-flip channel (black symbols), while scattering by phonons is non-spin flip (open symbols) (taken from Paolasini *et al.* (1996)). The line is simply to guide the eye. See text for details.

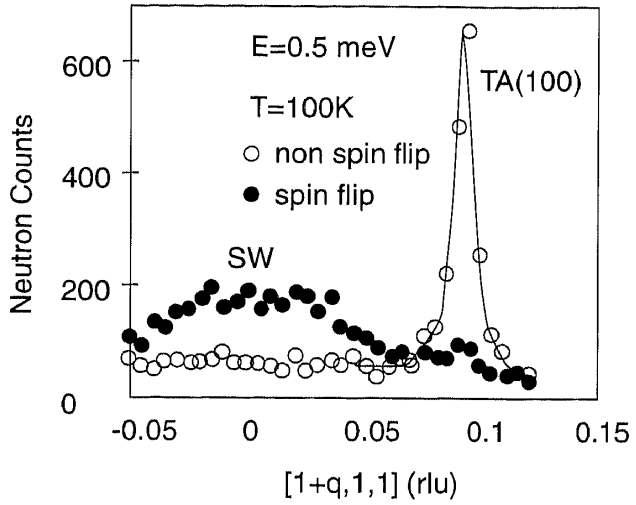

Longitudinal polarimetry is not only an important method for measuring magnetic and nuclear cross sections unambiguously; it is also very powerful in separating self- and collective dynamics in materials that contain strong incoherent scatterers like hydrogen in biological materials and polymers (Cook *et al.*, 1990) (see §7).

The XYZ Method

The longitudinal polarimetry method can be generalised to polarisation analysis along the three Cartesian directions, the so-called XYZ method (that is, however, to be distinguished from spherical polarimetry). This method makes it possible to apply the technique of polarisation analysis to time-of-flight spectrometers with multidetectors. With the coordinate system shown in Fig. 11, the non-spin-flip (NSF) and spin-flip (SF) cross sections are given by (Schärpf and Capellmann, 1993)

$$\sigma^x_{NSF} = \frac{1}{3}\sigma_{NS} + \frac{1}{2}\sigma_M \sin^2\alpha + \sigma_N \qquad (22)$$

Figure 11 Geometry of the XYZ polarisation method. P_i and P_f are the polarisations of the incident and scattered beams, respectively. **Q** is the scattering vector.

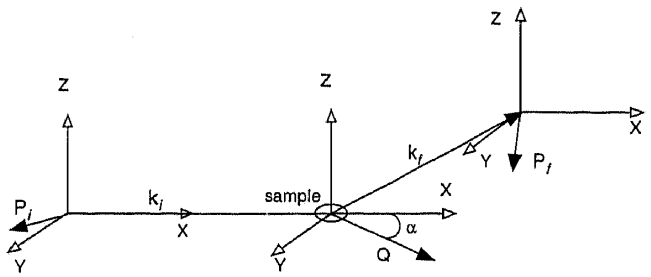

$$\sigma^{y}_{NSF} = \frac{1}{3}\sigma_{NS} + \frac{1}{2}\sigma_M \cos^2\alpha + \sigma_N \quad (23)$$

$$\sigma^{z}_{NSF} = \frac{1}{3}\sigma_{NS} + \frac{1}{2}\sigma_M + \sigma_N \quad (24)$$

$$\sigma^{x}_{SF} = \frac{2}{3}\sigma_{NS} + \frac{1}{2}\sigma_M(1+\cos^2\alpha) \quad (25)$$

$$\sigma^{y}_{SF} = \frac{2}{3}\sigma_{NS} + \frac{1}{2}\sigma_M(1+\sin^2\alpha) \quad (26)$$

$$\sigma^{z}_{SF} = \frac{2}{3}\sigma_{NS} + \frac{1}{2}\sigma_M, \quad (27)$$

where σ_M is the magnetic, σ_{NS} is the nuclear spin incoherent and σ_N is the coherent plus isotopic incoherent nuclear scattering cross section. The magnetic scattering can be isolated by combining these equations in the following way (independent of the angle α)

$$\frac{1}{2}\sigma_M = 2\sigma^{z}_{NSF} - \sigma^{y}_{NSF} - \sigma^{x}_{NSF} \quad (28)$$

$$= \sigma^{x}_{SF} + \sigma^{y}_{SF} - 2\sigma^{z}_{SF}. \quad (29)$$

The XYZ method has been applied successfully in determining the dynamical magnetic response in metals with small magnetic moments like V_2O_3 (Taylor *et al.*, 1999) and in probing both atomic and spin correlations, e.g., in spin glasses (Murani *et al.*, 1999) or magnetic defects in disordered alloys. A full account of the applicability of the XYZ technique to this problem has been recently reviewed by Cywinski *et al.* (1999, and references therein). Another important application of the XYZ method is that it makes it possible to separate incoherent and coherent atomic motions, as presented in §7.

Paramagnetic Scattering

According to the Rhodes and Wohlfarth (1963) theory, magnetic materials with *d* electrons can be classified in localised and itinerant systems. While for systems with localised spin densities, the magnetic moment in the paramagnetic phase is temperature independent, the ratio between paramagnetic and ordered moments varies with temperature in the Stoner model. The theory of spin fluctuations for localised and itinerant magnetic systems is reasonably well developed in the paramagnetic phase (Moriya, 1985). In that respect, inelastic scattering of neutrons provides direct experimental information on the spectrum of spin fluctuations on an absolute scale as it gives access to the space and time variation of the spin–spin correlation function $S(\mathbf{Q},\omega)$ that is related to the imaginary part of the dynamical susceptibility $\chi(\mathbf{Q},\omega)$ (Lovesey, 1984). Paramagnetic scattering is usually very weak and difficult to separate from coherent (phonons) and incoherent nuclear scattering. However, the signal can be uniquely identified in experiments by using the difference method, namely, the difference between the spin-flip scattering as measured in a (small) field parallel to Q and that perpendicular to Q contains only magnetic scattering (Squires, 1978; Ziebeck and Brown, 1980), the reason being that the inelastic scattering from phonons is suppressed and nuclear incoherent scattering and room background cancel. This statement is generally valid as long as the nuclear magnetic moments are disordered, i.e., $\langle I_x^2\rangle = \langle I_y^2\rangle = \langle I_z^2\rangle = \frac{1}{3}I(I+1)$, and $\langle I_\alpha\rangle = 0$. Nuclear ordering occurs only for extremely low temperatures (Siemensmeyer *et al.*, 1997).

Therefore one obtains, for example,

$$\frac{1}{2}\left[\frac{d^2\sigma}{d\omega\, d\Omega}\right]_m = \left[\frac{d^2\sigma^{+,-}}{d\omega\, d\Omega}\right]_{\parallel} - \left[\frac{d^2\sigma^{+,-}}{d\omega\, d\Omega}\right]_{\perp}$$

$$= \left[\frac{d^2\sigma^{+,+}}{d\omega\, d\Omega}\right]_{\perp} - \left[\frac{d^2\sigma^{+,+}}{d\omega\, d\Omega}\right]_{\parallel}. \quad (30)$$

Once the intensity of the paramagnetic fluctuations is measured, the *E*-integrated intensity can be put on an absolute scale by comparison with an acoustic phonon measured close to a Bragg peak (Ishikawa *et al.*, 1985) or by using an incoherent scatterer like vanadium. Hence, an effective, paramagnetic moment can be found, defined by

$$M(q) = \frac{1}{f(q)}\left[\int_0^\infty S(q,\omega)d\omega\right]^{1/2}, \quad (31)$$

where $f(q)$ is the form factor (Ziebeck and Brown, 1980). Ishikawa *et al.* (1985) pointed out that Eq. (31) overestimates the amplitude of spin fluctuations at low temperatures when the energy range of the spin fluctuations extends beyond $\sim k_B T_c$. They propose instead to use the Kramers–Kronig relation to obtain first the static susceptibility that is linked via the fluctuation–dissipation theorem to the amplitude of the spin fluctuations through $\langle M^2(q)\rangle = 3k_B T\chi(q)$ for $\hbar\omega \ll k_B T$ and

$$\chi(q) = g^2\mu_B^2 \int_{-\infty}^{\infty} \frac{S(q,\omega)[1-\exp(-\hbar\omega/k_B T)]}{\hbar\omega} d\omega. \quad (32)$$

Measurements of the paramagnetic fluctuations in MnSi with a coarse energy resolution (so that the *E* integration is automatically performed) with Eq. (31) (Ziebeck and Brown, 1980) and Eq. (32) (Ishikawa *et al.*, 1985) show that the amplitude of the local magnetic moment indeed increases with increasing temperature, in agreement with self-consistent renormalisation theory (Fig. 12) (Moriya, 1985).

Using the difference technique, the scaling behaviour of many different itinerant ferromagnets has been investigated in the paramagnetic phase and it was shown that the scattering functions of Fe and Ni can be modelled above T_c by a simple Lorentzian scattering function given by (Wickstead *et al.*, 1984)

$$S(q,\omega) = \frac{\omega}{1-\exp(-\omega/T)}\chi(q=0)\frac{\kappa^2}{\kappa^2+q^2}\frac{\Gamma_q}{\Gamma_q^2+\omega^2}, \quad (33)$$

Figure 12 Temperature dependence of $4\pi q^2\langle M_q^2\rangle$ plotted against q in MnSi as measured with polarised neutrons by Ishikawa *et al.* (1985). It is apparent from the figure that the mean-square amplitude of the spin fluctuations increases with increasing temperature in agreement with the calculations of the self-consistent renormalisation theory (Moriya, 1985).

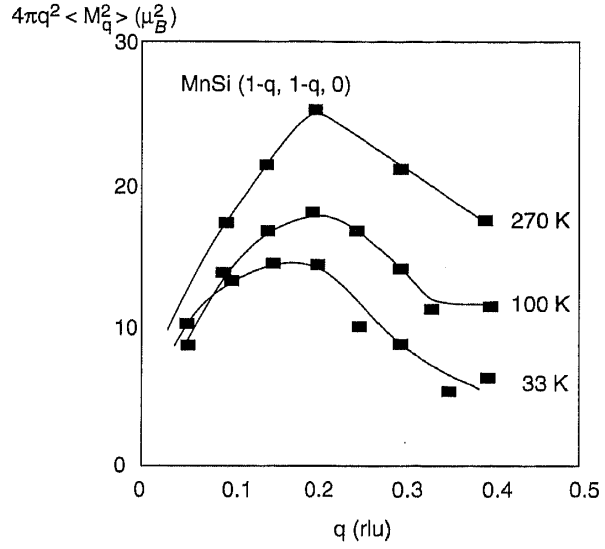

where the inverse correlation length $\kappa = \kappa_0(T/T_c - 1)^{0.7}$, the line width $\Gamma_q = Aq^{2.5}f(\kappa/q)$ and $f(x)$ is approximately given by the Résibois–Piette scaling function (Résibois and Piette, 1970).

To conclude, polarised neutron scattering is a powerful method for measuring paramagnetic fluctuations in particular when the signal is weak.

Transverse and Longitudinal Excitations in Ferromagnets

The magnetic properties of compounds with localised spin densities are usually described by the Heisenberg Hamiltonian

$$H = -\sum_{i,j} J_{ij}\mathbf{S}_i \cdot \mathbf{S}_j, \qquad (34)$$

where J_{ij} is the exchange integral between the spins located at the i and j positions, respectively (Fazekas, 1999). Depending on the sign of the exchange integral, Eq. (34) favours either antiferromagnetic or ferromagnetic ground states. If exchange interactions extend beyond nearest neighbours, competing effects can occur that may lead to noncollinear or even incommensurate magnetic structures.

Because of its simplicity, the Heisenberg ferromagnet is often taken as a model system for studying the properties of phase transitions. Within the simple picture of localised spins, long-range order is lost due to the thermal excitation of spin waves that evolve into the critical scattering at T_c. Using unpolarised neutron scattering the spin dynamics close to T_c has been investigated in detail (Passell *et al.*, 1978). It was shown that the spin waves, i.e., the spin fluctuations transverse to the magnetisation vector **M**, renormalise close to T_c and that the susceptibility $\chi(q)$ as measured at small angles diverges at small q for $T \to T_c$. Here, q is the reduced momentum transfer with respect to the nearest Bragg peak. The divergence of $\chi(q)$ is due to longitudinal fluctuations along **M** because the cross section for spin waves does not contain a correlation length that diverges at T_c. Unpolarised neutron scattering was not successful in detecting the longitudinal fluctuations in ferromagnets in contrast to the situation in antiferromagnets (Horn *et al.*, 1978; Coldea *et al.*, 1998), where they can be easily observed.

The longitudinal fluctuations can be isolated by means of inelastic neutron scattering with polarisation analysis (Böni *et al.*, 1990, 1991). The experiment is performed by measuring the differential spin-flip and non-spin-flip cross sections from a ferromagnetic sample, for example, EuS, that is saturated in a vertical magnetic field B_v that is perpendicular to the scattering vector **Q**. Figure 13 shows three typical measurements on EuS that have been performed longitudinal and transverse to the reciprocal lattice point (200) at 0.93 T_c (Böni *et al.*, 1995, 1997).

The spin-flip data show the spin waves with polarisation vectors $\delta\mathbf{S}$ transverse and parallel to the reduced momentum transfer **q**. The former are the Goldstone modes of the system and diverge like $\chi^T_{sw} \propto 1/q^2$ (Table 3). The longitudinal spin waves attain a mass (Fisher and Aharony, 1973a,b) due to the dipolar interactions and do not diverge, $\chi^L_{sw} \propto 1/(q^2 + q_D^2)$.

Figure 13 Constant-**Q** scans probing magnetic fluctuations in the ferromagnetic phase of EuS. The solid lines are fits to the data using Lorentzian spectral weight functions convoluted with the resolution function of the spectrometer IN14 at the ILL. The longitudinal spin waves are reduced in intensity due to the dipolar interactions. The parallel fluctuations are quasielastic.

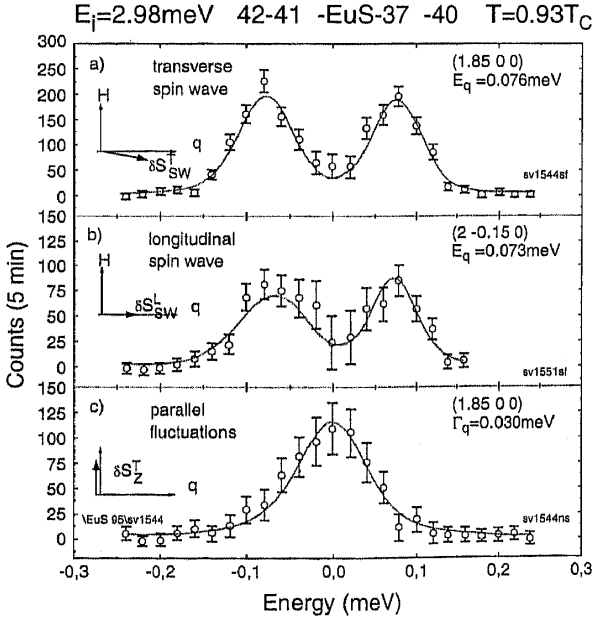

Finally the non-spin-flip data show the longitudinal fluctuations that are quasielastic and diverge like $\chi_z \propto 1/(q^2+\kappa^2)$. Because the width Γ_q of $\chi_z(q,\omega)$ is comparable to the spin wave energy E_q it is clear why the longitudinal fluctuations escaped detection with unpolarised neutron scattering. The results are in qualitative and quantitative agreement with a coupled mode analysis (Lovesey, 1993) and mode–mode coupling theory (Schinz and Schwabl, 1998).

Spin Waves and Phasons in Incommensurate, Antiferromagnetic Cr

One of the outstanding features of antiferromagnetic Cr is the occurrence of an incommensurate spin-density wave below $T_N = 311$ K that is transversely polarised (S perpendicular to $Q^{\pm}$) with $Q^{\pm} = (1 \pm \delta, 0, 0)$ being the incommensurate wave vector (for a review, see Fawcett (1988)). The magnetic excitations exhibit many unusual features that are not well understood. In particular, the magnetic modes that originate from the magnetic satellite peaks at $Q^{\pm}$ have such a steep dispersion that the creation and annihilation peaks cannot be resolved anymore. Using inelastic scattering of unpolarised neutrons and analysing the width of the peaks in constant energy scans led to the conclusion that the velocity of the excitations is $c_{sw} \simeq 1020$ meVÅ (Als-Nielsen *et al.*, 1971). This value deviates significantly from the theoretical value of a random phase approximation (RPA) that is given by $c_{sw}^{th} = \sqrt{\frac{1}{3}}v_F \simeq 1500$ meVÅ, where v_F is the Fermi velocity (Fishman and Liu, 1996a,b). When unpolarised neutron scattering is used, it has been shown that transverse (with respect to the staggered magnetisation) and longitudinal excitations contribute to the inelastic scattering that emerges from the incommensurate $Q^{\pm}$ satellite peaks (Lorenzo *et al.*, 1994).

In the absence of sizable magnetic–nuclear interference contributions in the cross section, the most direct way of separating the transverse from the longitudinal fluctuations is the use of longitudinal polarimetry. For such an experiment it is necessary to use a Cr single crystal cooled through T_N in a large magnetic field in order to induce a single-Q state. During the experiment, a vertical field B = 4 T was applied along [0 0 1] in order to enforce a single-domain spin-density wave with the magnetic moments aligned along the [0 1 0] direction. In this configuration, the spin-flip scattering is due to the longitudinal modes and the non-spin-flip scattering due to the transverse modes.

Figure 14 shows constant energy scans for $E = 4.2$ meV measured in the transverse spin-density wave phase at $T = 230$ K (0.74 T_N) (Böni *et al.*, 1998). It is clearly seen that the inelastic, incommensurate peaks with transverse polarisation are significantly sharper than the corresponding longitudinal peaks. Therefore, the mode velocity of the spin waves, c_{sw}, is significantly larger than the mode velocity of the phason modes, c_{ph}. These results are in qualitative agreement with results of RPA theory (Fishman and Liu, 1996a,b). In addition, the data show that the enhanced magnetic scattering at [1 0 0] and $E = 4.2$ meV has a longitudinal polarisation. Without going into further details the results indicate that a proper understanding of the magnetic excitations in Cr can only be gained if polarisation analysis is used.

Table 3 Transverse and Longitudinal Susceptibilities of a Heisenberg Ferromagnet with Dipolar Interactions in the Ordered and Paramagnetic Phases for Different Directions of the Momentum Transfer **q** and Accessible by One-Dimensional Polarisation Analysis (taken from Böni *et al.* (1997)).

	$T < T_c$	$T > T_c$
$\mathbf{M} \parallel \mathbf{q}$	$\frac{2}{q^2} + \frac{1}{q^2+\kappa_z^2+q_D^2}$	$\frac{2}{q^2+\kappa^2} + \frac{1}{q^2+\kappa_z^2+q_a^2}$
$\mathbf{M} \perp \mathbf{q}$	$\frac{1}{q^2} + \frac{1}{q^2+q_D^2} + \frac{1}{q^2+\kappa_z^2}$	$\frac{2}{q^2+\kappa^2} + \frac{1}{q^2+\kappa_z^2+q_a^2}$

Figure 14 Constant-E scans at 4.2 meV, probing the longitudinal and transverse excitations along the [100] direction in the transverse spin-density-wave phase of Cr at $T = 230$ K. The inset shows the intersection of the constant-E scan with the dispersion of the transverse (solid lines) and the longitudinal modes (broken lines) and the Fincher–Burke modes.

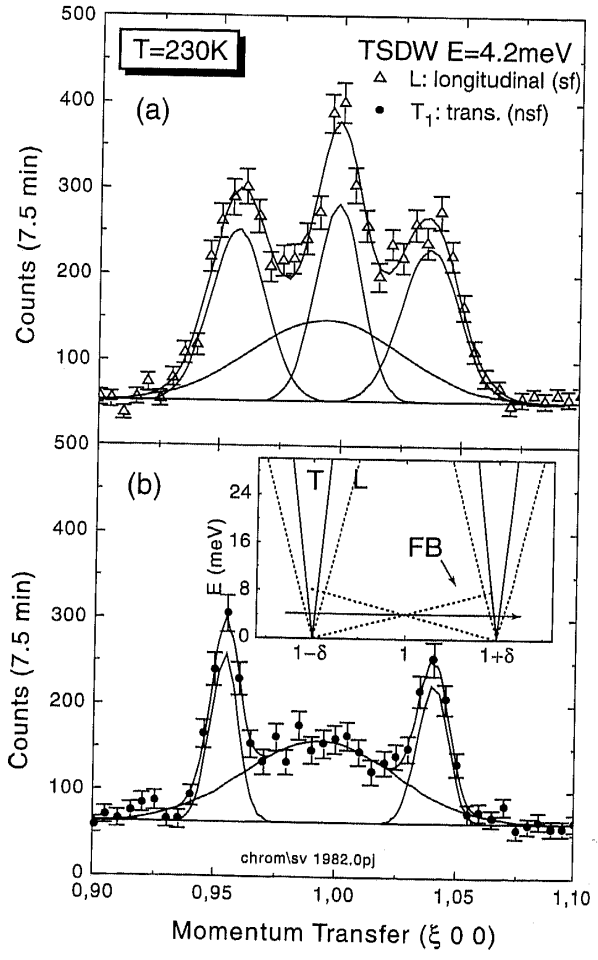

Magnetic Excitations in a Heavy Fermion Superconductor

The heavy fermion superconductor UPd_2Al_3 exhibits the unusual coexistence of antiferromagnetism and superconductivity below $T_c = 2$ K, i.e. the ordered magnetic moments of the *f* electrons of *U* persist in the superconducting phase (Geibel *et al.*, 1991). This has been taken as a sign that the interplay of magnetism and superconductivity could be studied in this material. Neutron (Krimmel *et al.*, 1992) and X-ray scattering (Gaulin *et al.*, 1994) experiments have shown that the magnetic structure of UPd_2Al_3 consists of ferromagnetic planes stacked along the *c* axis with a propagation vector $Q_0 = (0, 0, 0.5)$. The magnetic moments are confined within the hexagonal plane and are found to have an unusually large value of $\mu = 0.85\mu_B$ at saturation. First elastic (Krimmel *et al.*, 1993; Kita *et al.*, 1994) and inelastic (Petersen *et al.*, 1994) neutron scattering experiments could not unambiguously reveal any change in the magnetic properties of UPd_2Al_3 upon cooling the sample below the superconducting transition temperature.

Inelastic neutron scattering experiments (Sato *et al.*, 1997; Metoki *et al.*, 1998) performed with an improved energy resolution as compared to the work of Petersen *et al.* showed that there exist two contributions to the spectrum of magnetic fluctuations in UPd_2Al_3. While the first one corresponds to the spin-wave previously measured by Petersen *et al.* a second mode localised around the antiferromagnetic wave vector Q_0 is observed in the energy range $0 < E < 0.5$ meV. This lower energy mode is heavily damped for all temperatures in the antiferromagnetically ordered phase and strongly sharpens upon passing into the superconducting phase. At the lowest temperature the low-energy mode develops an apparent energy gap with a value comparable to T_c (Bernhoeft *et al.*, 1998a; Metoki *et al.*, 1998). Further evidence of a strong interplay between magnetic fluctuations and superconductivity in this compound originates from the use of polarised neutrons as shown in Fig. 15. Using a polarised beam, it was possible to show that the two magnetic modes are both polarised transverse to the magnetisation vector and hence are likely to interact with each other (Bernhoeft *et al.*, 1998b).

To perform this experiment the sample was field-cooled, so that the magnetic domains could be aligned along the magnetisation vector **M**. Using a neutron polarisation perpendicular to the scattering plane, it turns out that magnetic fluctuations parallel to the magnetisation are non-spin flip, while those perpendicular to **M** appear in the spin-flip channel. Analysis of the line shape of the inelastic neutron scattering data suggests that *f* electrons located in a small energy range around the Fermi surface play a significant role in forming the superconducting state in UPd_2Al_3 (Bernhoeft *et al.*, 2000).

Figure 15 Experimental data from UPd_2Al_3 at the antiferromagnetic wave vector $\mathbf{Q}_0 = (0, 0, 0.5)$ and $T = 150$ mK. The data were taken with a fixed outgoing neutron wave vector of $k_f = 1.15\text{Å}^{-1}$. Frames (a) and (b) are taken with polarised neutrons. For means of comparison a scan measured with unpolarised neutrons is shown in frame (c). In frames (a) and (b), the transverse response is shown as black symbols, whereas the longitudinal component is represented by open circles. See Bernhoeft *et al.* (1998b) for details.

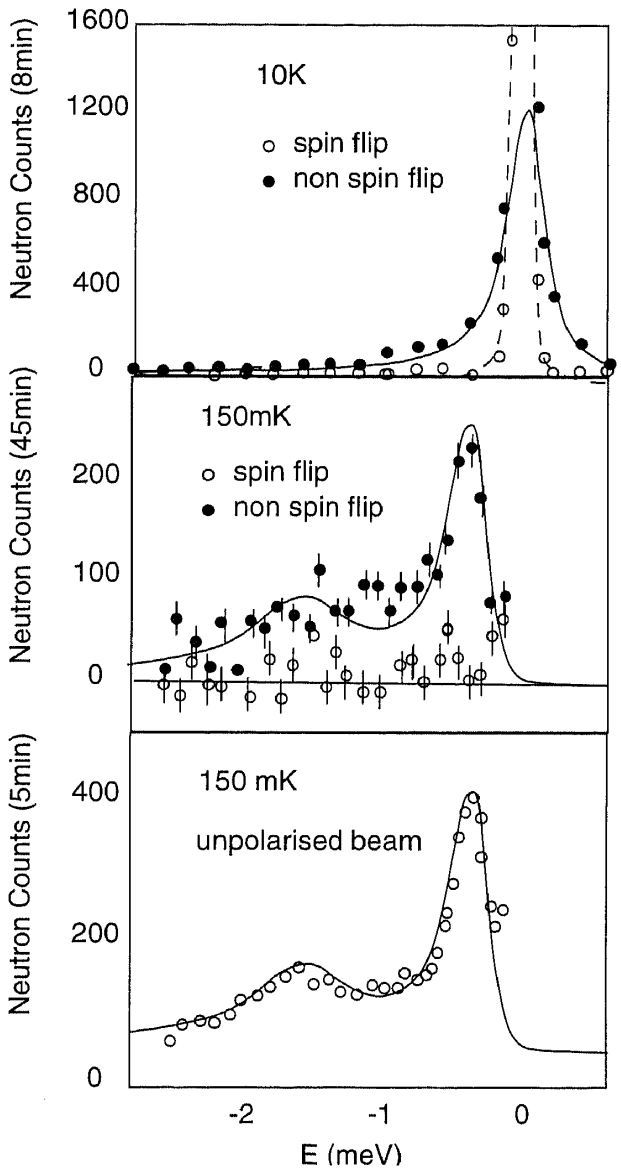

Magnons and Solitons in Low-Dimensional Systems

The magnetic properties of low-dimensional compounds have attracted a lot of attention as new effects due to quantum fluctuations are strong. For one-dimensional Heisenberg antiferromagnets the ground states and energy excitations are different for integer and half-integer spins (Haldane, 1983a,b). Antiferromagnetic chains with $S = 1/2$ spins have a disordered

ground state. The low-lying excitations are characterised by a continuum of excitations without energy gap at the zone centre. On the other hand, for integer spins a finite energy gap was predicted by Haldane and obtained by numerical calculations (Haldane, 1983a,b; Affleck, 1989). Examples of materials exhibiting a Haldane gap are NENP (Regnault *et al.*, 1994, and references therein), Y_2BaNiO_5 (Darriet and Regnault, 1993), or $CsNiCl_3$ (Enderle *et al.*, 1999, and references therein). The characteristics expected for a Haldane system have been observed in these compounds by inelastic neutron scattering, like (i) a periodicity of 2π in the magnon dispersion, (ii) linewidth broadening of the magnetic excitations as a function of momentum transfer indicating the presence of a two-magnon continuum and (iii) a large field dependence of the magnetic excitations (Regnault and Renard, 1997).

Polarised neutron scattering experiments have shown that the energy gap in the spectrum of magnetic excitations in $CsNiCl_3$ is a triplet (Steiner *et al.*, 1987). In such quasi-one-dimensional antiferromagnets, weak interchain exchange interactions J' can lead to a Néel phase at low temperatures. In fact the ordering temperature depends on the ratio of the intrachain interactions J to J'. Interestingly, for such systems, where antiferromagnetic ordering is close to disorder, linear spin-wave theory does not account properly either for the energy dependence of the magnetic excitations or for the number of magnetic modes. In particular, the existence of a longitudinally polarised magnetic mode that cannot be predicted by standard or modified spin-wave theory has been proven by means of inelastic polarised neutron scattering in $CsNiCl_3$ (Enderle *et al.*, 1999, and references therein) and Nd_2BaNiO_5 (Fig. 16) (Raymond *et al.*, 1999). The instrumental setup was chosen so that magnetic excitations transverse to the magnetic moments could be separated from the fluctuations along the spin direction. With such a geometry, it could be shown that additional excitations with longitudinal polarisation are present in the spectrum of $S(\mathbf{Q},\omega)$, in agreement with calculations based on renormalisation-group theory (Affleck and Wellman, 1992).

The quasi-one-dimensional $S = 1/2$ inorganic compound $CuGeO_3$ presents the particularity to undergo a chemical phase transition below $T = 14$ K to a phase, called *spin-Peierls* phase, where the copper chain is dimerised (Hase *et al.*, 1993; Pouget *et al.*, 1994). Consequently, the exchange interactions along the chain direction are not uniform anymore but alternate with values J and J', respectively. The magneto-elastic interaction is presumably responsible for this phase transition characterised by a nonmagnetic ground

Figure 16 Temperature dependence of constant **Q**-scans measured in Nd_2BaNiO_5 with polarised neutrons. Open and black circles refer to spin-flip and non-spin-flip scattering, respectively (taken from Raymond *et al.* (1999)).

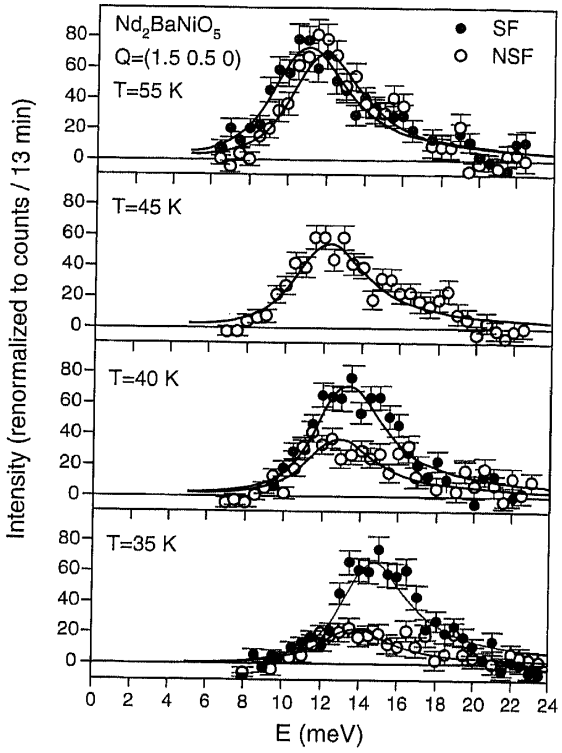

state. For such a system, the spectrum of magnetic excitations attains a gap at the zone centre, whereas the first excited states are triplets. In $CuGeO_3$ the gap has a value of $\Delta \sim 2.5$ meV (Nishi *et al.*, 1996) while away from the zone centre, the spectrum of magnetic fluctuations is strongly dispersive along the copper chain direction. High-resolution inelastic polarised-neutron experiments, however, revealed that there is a second energy gap in this compound that separates the low-energy magnon-like mode from a continuum of excitations extending to higher energies (Aïn *et al.*, 1997; Lorenzo *et al.*, 1997). The occurrence of two energy gaps in the spectrum of magnetic excitations in $CuGeO_3$ is clearly a signature of strong quantum fluctuations in $S = 1/2$ antiferromagnetic chains. This behaviour differs drastically from one-dimensional systems with large spin number S that in some cases can be described by the classical sine-Gordon equation. The combined effects of nonlinearity and dispersion in these systems lead, in addition, to the linear excitations, to a special class of excitations called "solitons" (Steiner *et al.*, 1987).

In a ferromagnetic chain, an excitation of soliton-type can be viewed as a 2π turn of the spins over a small distance, in a similar way to a domain wall that would propagate through the crystal. These excitations are accessible to inelastic neutron scattering and in particular to polarised neutrons that make it possible to measure selectively the different space

and time correlation functions $S^{x,x}(Q,\omega)$, $S^{y,y}(Q,\omega)$ and $S^{z,z}(Q,\omega)$ (Steiner *et al.*, 1987). Although experiments with unpolarised neutrons have shown strong evidence of nonlinear excitations in the chain compounds $CsNiF_3$ and TMMC, a crucial test for the existence of solitonic excitations is the measurement of the components fluctuating along and perpendicular to an applied magnetic field (Steiner *et al.*, 1983; Mikeska and Steiner, 1991; Steiner, 1995).

By separating the longitudinal part $S^{\parallel}(Q,\omega)$ of the dynamic structure factor from the transverse part $S^{\perp}(Q,\omega)$ with longitudinal polarimetry analysis (see Fig. 17), Boucher *et al.* (1986) were able to study the wave vector and energy dependence of solitonic fluctuations in the antiferromagnetic chain compound $(CD_3)_4NMnCl_3$(TMMC). This study led to the result that amplitude and lifetime of the solitons are strongly affected by collisions with magnons and by mutual interactions. As a consequence, the lineshape and the linewidth of the experimental dynamical susceptibility differ from the actual theoretical calculations based upon the low-density noninteracting soliton gas model (Steiner *et al.*, 1987).

§7. Self- and Collective Diffusive Atomic Motions

Collective motions of light atoms in metals consist of two different processes (Sinha and Ross, 1988). The first one can be viewed as pure diffusion of ions through the lattice while the second process involves cooperative hopping of mutually interacting particles. Hence, the neutron scattering functions contain incoherent and coherent scattering contributions that are given within the random phase approximation by Lorentzian functions centred around zero energy transfer

$$S_{\mathrm{inc}}(Q,\omega) = \frac{1}{\pi}\frac{D_t Q^2}{(D_t Q^2)^2+\omega^2}$$

$$S_{\mathrm{coh}}(Q,\omega) = \frac{S(Q)}{\pi}\frac{D_c Q^2}{(D_c Q^2)^2+\omega^2}. \qquad (35)$$

$S(Q)$ is the static structure factor and D_t and D_c are the coefficients of incoherent and coherent diffusion, respectively.

To separate the two quasi-elastic scattering processes that appear simultaneously in the neutron spectrum, it is best to use polarisation analysis. In analogy to paramagnetic scattering, coherent and incoherent processes can be isolated by calculating the difference between non-spin-flip and spin-flip scattering. In the case of different isotopes and disordered nuclear spins, the matrix elements for non-spin-flip and spin-flip scattering are given for the coherent cross section by

$$\sigma^{++}_{\mathrm{coherent}} = \sigma^{--} = \langle N\rangle^2_{\mathrm{iso}} \qquad (36)$$

$$\sigma^{+-}_{\mathrm{coherent}} = \sigma^{-+} = 0 \qquad (37)$$

and for the incoherent scattering by (Squires, 1978)

$$\sigma^{++}_{\mathrm{incoherent}} = \sigma^{--}_{\mathrm{incoherent}} = \langle N^2\rangle_{\mathrm{iso}} - \langle N\rangle^2_{\mathrm{iso}} + \frac{1}{3}\langle B^2 I(I+1)\rangle_{\mathrm{iso}} \qquad (38)$$

$$\sigma^{+-}_{\mathrm{incoherent}} = \sigma^{-+}_{\mathrm{incoherent}} = \frac{2}{3}\langle B^2 I(I+1)\rangle_{\mathrm{iso}}, \qquad (39)$$

where $\langle\cdots\rangle_{\mathrm{iso}}$ refers to isotopic averaging and I to the nuclear spin (Squires, 1978). In compounds that contain scatterers with one isotope only, the coherent cross section is obtained by dividing the spin-flip scattering by 2 and subtracting the result from the non-spin-flip intensity. In this case, all the incoherent scattering is spin-flip scattering. Figure 18 shows

Figure 17 Spectra of magnetic excitations measured in TMMC with inelastic polarised neutron scattering showing that the transverse and longitudinal fluctuations are different. See text and Boucher *et al.* (1986) for details.

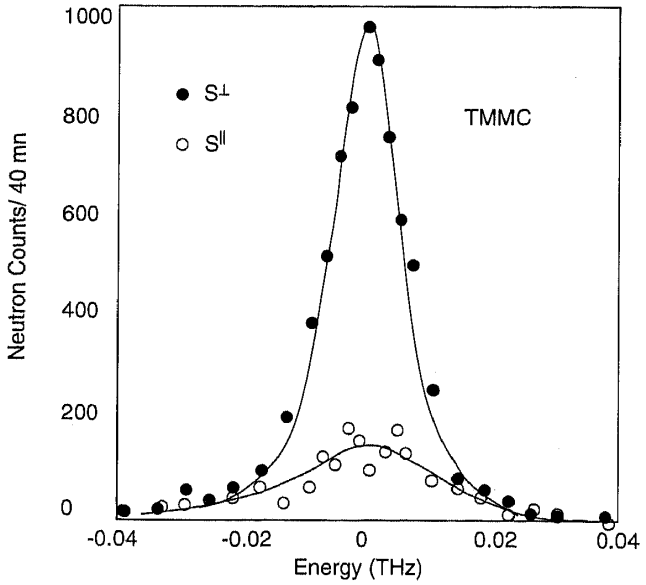

Figure 18 Coherent and incoherent scattering processes observed and calculated in α′-$NbD_{0.7}$ by means of polarised neutron scattering on the multicounter time-of-flight spectrometer D7 at the ILL (taken from Cook *et al.* (1990)).

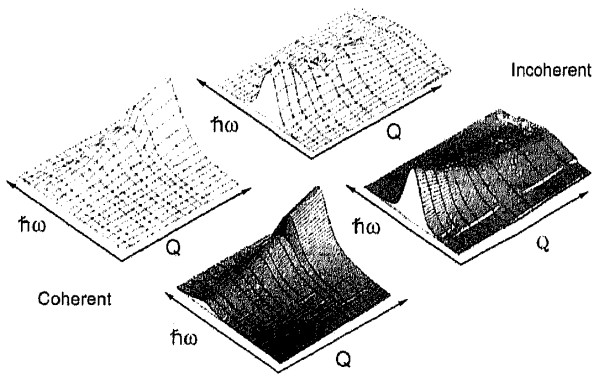

the results of measurements of the self- and collective dynamics of deuterium in a single crystal of Nb using the time-of-flight spectrometer D7 at ILL (Cook *et al.*, 1990). It is clear that polarisation analysis gives an unambiguous separation of the incoherent and coherent quasi-elastic signals over a large range of momentum transfers Q. Such a study makes it possible to determine distance and direction of jump processes, hopping and residential times through the analysis of the Q-dependence and energy width of the Lorentzian functions in Eqs. (35).

§8. Conclusions

The examples given in the previous sections have shown that neutron scattering with polarised neutrons has become a very important means for measuring magnetic properties over a wide range of Q and ω and for distinguishing between coherent and incoherent excitations in materials. Most experiments with polarised neutrons are being performed up to now at sources providing continuous neutron beams. The main reason being that most neutron polarisers are more ideally suited for applications with constant wavelength. The recent advances in the field of supermirrors and ^{3}He filters have improved the situation. These new devices make it possible to extend polarisation analysis to high neutron energies and to use large area detectors. Therefore, we expect that polarisation analysis will also soon become a standard technique at pulsed neutron sources.

Recently, new developments in the field of magnetism that rely strongly on new developments in polarised neutron scattering have emerged. As a first example, we mention systems that can be characterised by sets of exponents that differ according to the space and spin dimensionality and hence can be grouped into universality classes. In frustrated spin systems, the order parameter includes a term describing the spin chirality $\mathbf{C} = [\mathbf{S}_1 \times \mathbf{S}_2]$. A direct observation of the fluctuations of the chiral variable is, however, impossible with unpolarised neutron scattering as these are related to four-spin correlation functions. Because the chiral part of the neutron cross section is polarisation dependent (Maleyev, 1995) it can be observed with polarisation analysis.

As a second example, we mention that the Cryopad technique opens the possibility of applying spherical neutron polarimetry in inelastic neutron scattering as it makes it possible to measure the nuclear–magnetic interference term directly. Recently, Maleyev (1999) has reconsidered the implication of the nuclear–magnetic interference term (NMIT) for inelastic scattering and has shown that in analogy with elastic scattering, it leads to a dependence of the neutron cross section upon $\mathbf{P}_i$, namely to a finite polarisation of the scattered neutrons and to a rotation of the initial polarisation. In particular, Maleyev has shown that the part of the dynamical susceptibility due to the NMIT is nonzero if there is a spin–lattice interaction characterised by an axial vector, as is the case, e.g., for the Dzialoshinskii–Moriya (DM) interaction $\mathbf{D} \cdot [\mathbf{S}_i \times \mathbf{S}_j]$. Indications of the importance of the DM interaction in the spin–lattice coupling and hence of its accessibility through inelastic spherical neutron polarimetry originates from recent inelastic experiments performed in the spin-Peierls compound $CuGeO_3$ where a rotation of the final polarisation $\mathbf{P}_f$ has been detected when the incident polarisation is chosen parallel to the scattering vector (Regnault *et al.*, 1999). Such measurements have shown that spherical neutron polarimetry can be applied in the field of inelastic neutron scattering, although counting times are long due to poor statistics. A further application may be the study of magneto-elastic coupling, which plays an important rôle in invar alloys (Brown *et al.*, 1989). Together with new theoretical interest in such problems, it is probable that this method will contribute to an improved understanding of phase transitions, where spin–lattice interactions are important, as such effects cannot be studied by standard polarisation analysis.

References

Affleck, I. 1989, *J. Phys.: Condens. Matter* **1**, 3047.

Affleck, I. and Wellman, G. F. 1992, *Phys. Rev. B* **46**, 8934.

Aïn, M., Regnault, L. P., Dhalenne, G., Revcolevschi, A. and Jolicoeur, Th. 1997, *J. Appl. Phys.* **81**, 4393.

Als-Nielsen, J., Axe, J. D. and Shirane, G. 1971, *J. Appl. Phys.* **42**, 1666.

Anderson, I. S., Hamelin, B., Høghøj, P., Courtois, P. and Humblot, H. 2000, In *Proceedings of the Seventh School on Neutron Scattering, Frontiers of Neutron Scattering* (A. Furrer, Ed.), p. 44. World Scientific, Singapore.

Baron, V., Gillon, B., Kahn, O., Mathoniere, C., Bonnet, M. and Boucherle, J. X. 1993, *Mol. Cryst. Liquid Cryst.* **223**, 247.

Baron, V., Gillon, B., Plantevin, O., Cousson, A., Mathoniere, C., Kahn, O., Grand, A., Ohrstrom, L. and Delley, B. 1996, *J. Am. Chem. Soc.* **118**, 11,822.

Bednorz, J. G. and Müller, K. A. 1986, *Z. Physik B* **64**, 189.

Bernhoeft, N., Hiess, A., Roessli, B., Sato, N., Aso, N., Endoh, Y., Lander, G. H. and Komatsubara, T. 1998a, In *Itinerant Electron Magnetism: Fluctuations Effects* (D. Wagner, W. Brauneck and A. Solontsov, Eds.), p. 43. Kluwer Academic, Dordrecht.

Bernhoeft, N., Sato, N., Roessli, B., Aso, N., Hiess, A., Lander, G. H., Endoh, Y. and Komatsubara, T. 1998b, *Phys. Rev. Lett.* **81**, 4244.

Bernhoeft, N., Sato, N., Roessli, B., Aso, N., Hiess, A., Lander, G. H., Endoh, Y. and Komatsubara, T. 2000, *Physica B* **281–282**, 993.

Blume, M. 1963, *Phys. Rev. B* **130**, 1670.

Böni, P. 1996, *J. Neutron Res.* **5**, 63.

Böni, P., Martínez, J. L. and Tranquada, J. M. 1990, *J. Appl. Phys.* **67**, 5436.

Böni, P., Martínez, J. L. and Tranquada, J. M. 1991, *Phys. Rev. B* **43**, 575.

Böni, P., Hennion, M. and Martínez, J. L. 1995, *Phys. Rev. B* **52**, 10,142.

Böni, P., Roessli, B., Görlitz, D., Kötzler, J. and Martínez, J. L. 1997, *Proceedings of the IÆA Technical Committee Meeting on Neutron Beam Research, Lisbon*, p. 68.

Böni, P., Sternlieb, B. J., Shirane, G., Roessli, B., Lorenzo, J. E. and Werner, S. A. 1998, *Phys. Rev. B* **57**, 1057.

Böni, P., Clemens, D., Senthil Kumar, M. and Pappas, C. 1999, *Physica B* **267–268**, 320.

Boucher, J. P., Regnault, L. P., Pynn, R., Bouillot, J. and Renard, J. P. 1986, *Europhys. Lett.* **1**, 415.

Boucherle, J. X., Givord, D. and Schweizer, J. 1982, *J. Phys. Coll. C7* **43**, 199.

Boucherle, J. X., Henry, J. Y., Papoular, R. J., Rossat-Mignod, J., Schweizer, J., Tasset, F. and Uimin, G. 1993, *Physica B* **192**, 25.

Bouchiat, M. A., Carver, T. R. and Varnum, C. M. 1960, *Phys. Rev. Lett.* **5**, 373.

Brown, P. J. 1992, In *International Tables for Crystallography* Vol. C, p. 391. Kluwer Academic, Dordrecht.

Brown, P. J., Jassim, I. K., Neumann, K.-U. and Ziebeck, K. R. A. 1989, *Physica B* **161**, 9.

Brown, P. J., Forsyth, J. B. and Tasset, F. 1993, *Proc. R. Soc. London A* **442**, 147.

Brown, P. J., Forsyth, J. B. and Tasset, F. 1999, *Physica B* **267–268**, 215.

Cable, J. W., Wollan, E. O., Felscher, G. P., Brun, T. O. and Hornfeldt, S. P. 1975, *Phys. Rev. Lett.* **34**, 278.

Coldea, R., Cowley, R. A., Perring, T. G., McMorrow, D. F. and Roessli, B. 1998, *Phys. Rev. B* **57**, 5281.

Colgrove, F. D., Schearer, L. D. and Walker, K. 1963, *Phys. Rev.* **132**, 2561.

Cook, J. C., Richter, D., Schärpf, O., Benham, M. J., Ross, D. K., Hempelmann, R., Anderson, I. S. and Sinha, S. K. 1990, *J. Phys.: Condens. Matter* **2**, 79.

Courtois, P. 1999, *Physica B* **267–268**, 363.

Cywinski, R., Kilcoyne, S. H. and Stewart, J. R. 1999, *Physica B* **267–268**, 106.

Darriet, J. and Regnault, L. P. 1993, *Solid State Commun.* **86**, 409.

Delley, B. 1990, *J. Chem. Phys.* **92**, 508.

Delley, B. 2000, *J. Chem. Phys.* **113**, 7756.

Enderle, M., Tun, Z., Buyers, W. J. L. and Steiner, M. 1999, *Phys. Rev. B* **59**, 4235.

Fawcett, E. 1988, *Rev. Mod. Phys.* **60**, 209.

Fazekas, P. 1999, In *Lectures Notes on Electron Correlations and Magnetism*, Series in Modern Condensed Matter Physics, Vol. 5. World Scientific, Singapore.

Fisher, M. E. and Aharony, A. 1973a, *Phys. Rev. Lett.* **30**, 559.

Fisher, M. E. and Aharony, A. 1973b, *Phys. Rev. B* **8**, 3323.

Fishman, R. S. and Liu, S. H. 1996a, *Phys. Rev. Lett.* **76**, 2398.

Fishman, R. S. and Liu, S. H. 1996b, *Phys. Rev. B* **54**, 7252.

Freeman, A. J. and Desclaux, J. P. 1979, *J. Magn. Magn. Mater.* **12**, 11.

Gaulin, B. D., Gibbs, D., Isaacs, E. D., Lussier, J. G., Reimers, J. N., Schroder, A., Taillefer, L. and Zschack, P. 1994, *Phys. Rev. Lett.* **73**, 890.

Geibel, C., Schank, C., Thies, S., Kitazawa, H., Bredl, C. D., Bohm, A., Rau, M., Grauel, A., Caspary, R., Helfrich, R., Ahlheim, U., Weber, G. and Steglich, F. 1991, *Z. Phys. B* **84**, 1.

Gillon, B. and Schweizer, J. 1989, In *Molecules in Physics, Chemistry and Biology* (J. Marauni, Ed.), Vol. 3, p. 111. Kluwer Academic, Dordrecht.

Givord, D., Laforest, J., Schweizer, J. and Tasset, F. 1979, *J. Appl. Phys.* **50**, 2008.

Haldane, F. D. M. 1983a, *Phys. Lett. A* **93**, 464.

Haldane, F. D. M. 1983b, *Phys. Rev. Lett.* **50**, 1153.

Halpern, O. and Johnson, M. R. 1939, *Phys. Rev.* **55**, 898.

Hase, M., Teraski, I. and Uchinokura, K. 1993, *Phys. Rev. Lett.* **70**, 3651.

Heil, W., Dreyer, J., Hoffmann, D., Humblot, H., Lelièvre-Berna, E. and Tasset, F. 1999, *Physica B* **267–268**, 328.

Henry, J. Y., Papoular, R. J., Schweizer, J., Tasset, F., Uimin, G. and Zobkalo, I. 1994, *Physica C* **235–240**, 1659.

Høghøj, P. H., Anderson, I., Siebrecht, R., Graf, W. and Ben-Saidane, K. 1999, *Physica B* **267–268**, 355.

Horn, P. M., Hastings, J. M. and Corliss, L. M. 1978, *Phys. Rev. Lett.* **40**, 126.

Ishikawa, Y., Noda, Y., Uemura, Y. J., Majkrzak, C. F. and Shirane, G. 1985, *Phys. Rev. B* **31**, 5884.

Izyumov, Yu. A. and Maleev, S. V. 1962, *Sov. Phys. JETP* **14**, 1168.

Kahn, O. 1993, In *Molecular Magnetism*, VCH, Weinheim.

Kita, H., Dönni, A., Endoh, Y., Kakurai, K., Sato, N. and Kommatsubara, T. 1994, *J. Phys. Soc. Jpn.* **63**, 726.

Krimmel, A., Fischer, P., Roessli, B., Maletta, H., Geibel, C., Shank, C., Grauel, A., Loidl, A. and Steglich, F. 1992, *Z. Phys. B* **86**, 61.

Krimmel, A., Loidl, A., Fischer, P., Roessli, B., Dönni, A., Kita, H., Sato, N., Endoh, Y., Komatsubara, T., Geibel, C. and Steglich, F. 1993, *Solid State Commun.* **87**, 829.

Krist, Th., Müller, D. J. and Mezei, F. 1999, *Physica B* **267–268**, 194.

Lee, S. H. and Majkrzak, C. F. 1999, *Physica B* **267–268**, 341.

Lorenzo, J. E., Sternlieb, B. J., Shirane, G. and Werner, S. A. 1994, *Phys. Rev. Lett.* **72**, 1762.

Lorenzo, J. E., Regnault, L. P., Hennion, B., Aïn, M., Bourdarot, F., Kulda, J., Dhalenne, G. and Revcolevschi, A. 1997, *J. Phys. Condens. Matter* **9**, L211-17.

Lovesey, S. W. 1984, In *Theory of Neutron Scattering from Condensed Matter*, Vol. 2. Clarendon Press, Oxford.

Lovesey, S. W. 1993, *J. Phys. Condens. Matter* **5**, L251.

Maleyev, S. V. 1995, *Phys. Rev. Lett.* **75**, 4682.

Maleyev, S. V. 1999, *Physica B* **267–268**, 236.

Mannix, D., Coad, S., Lander, G. H., Rebizant, J., Brown, P. J., Paixão, J. A., Langridge, S., Kawamata, S. and Yamaguchi, Y. 2000, *Phys. Rev. B* **62**, 3801.

Mayers, J., Cywinski, R., Harris, I. R., Hixon, M. and Williams, W. G. 1986, In *Proc. Ninth Int. Conf. on Advanced Neutron Sources*, ICANS IX, SIN, Villigen, Switzerland.

Metoki, N., Haga, Y., Koike, Y. and Onuki, Y. 1998, *Phys. Rev. Lett.* **80**, 5417.

Mezei, F. 1972, *Z. Physik* **255**, 146.

Mezei, F. 1976, *Commun. Phys.* **1**, 81.

Mezei, F. and Dagleish, P. A. 1977, *Commun. Phys.* **2**, 41.

Mikeska, H. J. and Steiner, M. 1991, *Adv. Phys.* **40**, 191.

Mook, H. A. 1966, *Phys. Rev.* **148**, 495.

Moon, R. M. 1964, *Phys. Rev. A* **136**, 195.

Moon, R. M. 1982, *J. Phys. Coll. C7* **43**, 187.

Moon, R. M., Riste, T. and Koehler, W. C. 1969, *Phys. Rev.* **181**, 920.

Moriya, T. 1985, In *Spin Fluctuations in Itinerant Electron Magnetism*, Springer-Verlag, Berlin.

Murani, A. P., Schärpf, O., Andersen, K. H., Richard, D. and Raphel, R. 1999, *Physica B* **267–268**, 131.

Nathans, R., Shull, C., Shirane, G. and Andresen, A. 1959, *Phys. Chem. Solids* **10**, 138.

Newton, R. R. and Kittel, C. 1948, *Phys. Rev.* **74**, 1604.

Nishi, M., Fujita, O. and Akimitsu, J. 1996, *Phys. Rev. B* **50**, 1105.

Nunez, V., Brown, P. J., Forsyth, J. B. and Tasset, F. 1991, *Physica B* **174**, 60.

Paixão, J. A., Ramos Silva, M., Sorensen, S. A., Lebech, B., Lander, G. H., Brown, P. J., Langridge, S., Talik, E. and Goncalves, A. P. 2000, *Phys. Rev. B* **61**, 6176.

Paolasini, L., Lander, G. H., Shapiro, S. M., Caciuffo, R., Lebech, B., Regnault, L. P., Roessli, B. and Fournier, J. M. 1996, *Europhys. Lett.* **34**, 459.

Papoular, R. and Gillon, B. 1990a, *Europhys. Lett.* **13**, 429.

Papoular, R. and Gillon, B. 1990b, In *Neutron Scattering Data Analysis* (M. W. Johnson, Ed.), p. 101. Adam Hilger, Bristol.

Passell, L., Dietrich, O. W. and Als-Nielsen, J. 1976, *Phys. Rev. B* **14**, 4897, 4908, 4923.

Perdew, J. P. and Wang, Y. 1992, *Phys. Rev. B* **45**, 13244.

Petersen, T., Mason, T. E., Aeppli, G., Ramirez, A. P., Bucher, E. and Kleimann, R. N. 1994, *Physica B* **199–200**, 151.

Pontillon, Y., Ressouche, E., Romero, F., Schweizer, J. and Ziessel, R. 1997, *Physica B* **234–236**, 788.

Pouget, J. P., Regnault, L. P., Aïn, M., Hennion, B., Renard, J. P., Veillet, P., Dhalenne, G. and Revcolevschi, A. 1994, *Phys. Rev. Lett.* **72**, 4037.

Raymond, S., Yokoo, T., Zheludev, A., Nagler, S. E., Wildes, A. and Akimitsu, J. 1999, *Phys. Rev. Lett.* **82**, 2382.

Regnault, L. P. and Renard, J. P. 1997, *Physica B* **234–236**, 541.

Regnault, L. P., Zalyzniak, I., Renard, J. P. and Vettier, C. 1994, *Phys. Rev. B* **50**, 9174.

Regnault, L. P., Bourges, Ph. and Burlet, P. 1998, In *Neutron Scattering in Layered Copper-Oxide Superconductors* (A. Furrer, Ed.), p. 100. Kluwer Academic, Dordrecht.

Regnault, L. P., Tasset, F., Lorenzo, J. E., Roberts, T., Dhalenne, G. and Revcolevschi, A. 1999, *Physica B* **267–268**, 227.

Résibois, R. and Piette, C. 1970, *Phys. Rev. Lett.* **24**, 514.

Ressouche, E. 1999, *Physica B* **267–268**, 27.

Rhodes, P. and Wohlfarth, E. P. 1963, *Proc. R. Soc. A* **273**, 247.

Robinson, R. A., Lawson, A. C. S., Lynn, J. W. and Buschow, K. H. J. 1993, *Phys. Rev. B* **47**, 6138.

Sandratskii, L. M. and Kübler, J. 1995, *Phys. Rev. Lett.* **75**, 946.

Sato, N., Aso, N., Lander, G. H., Roessli, B., Komatsubara, T. and Endoh, Y. 1997, *J. Phys. Soc. Jpn.* **66**, 1884.

Schärpf, O. 1975, *J. Phys. E: Sci. Instrum.* **8**, 268.

Schärpf, O. and Capellmann, H. 1993, *Phys. Status Solidi A* **135**, 359.

Schinz, H. and Schwabl, F. 1998, *Phys. Rev. B* **57**, 8430, 8438, 8456.

Schweizer, J. 1995, In *Magnetic Neutron Scattering* (A. Furrer, Ed.), p. 70. World Scientific, Singapore.

Schweizer, J. 1997, *Physica B* **234–236**, 772.

Shirane, G., Cowley, R., Majkrzak, C. F., Sokoloff, J. B., Pagonis, B. and Perry, C. H. 1983, *Phys. Rev. B* **28**, 6251.

Shull, C. G. and Wedgwood, F. A. 1966, *Phys. Rev. Lett.* **16**, 513.

Shull, C. G. and Yamada, Y. 1962, *J. Phys. Soc. Jpn.* **17**, 1.

Siemensmeyer, K., Clausen, K. N., Lefmann, K., Lounasmaa, O. V., Metz, A., Nummila, K. K., Rasmussen, F. B., Steiner, M., Tuoriniemi, J. T. and Vuorinen, R. T. 1997, *Physica B* **234–236**, 768.

Sinha, S. K. and Ross, D. K. 1988, *Physica B* **149**, 51.

Squires, G. L. 1978, *Thermal Neutron Scattering*, Cambridge Univ. Press, Cambridge.

Stassis, C., Arthur, J., Majkrzak, C. F., Axe, J. D., Batlogg, B., Remeika, J., Fisk, Z., Smith, J. L. and Edelstein, A. S. 1986, *Phys. Rev. B* **34**, 4382.

Steiner, M. 1995, In *Magnetic Neutron Scattering* (A. Furrer, Ed.), p. 132. World Scientific, Singapore.

Steiner, M., Kakurai, K. and Kjems, J. K. 1983, *Z. Phys. B* **53**, 117.

Steiner, M., Kakurai, K., Kjems, J. K., Petitgrand, D. and Pynn, R. 1987, *J. Appl. Phys.* **61**, 3953.

Steinsvoll, O., Moon, R. M., Koehler, W. C. and Windsor, C. G. 1981, *Phys. Rev. B* **24**, 4031.

Stuhrmann, H. B. 1999, *Physica B* **267–268**, 92.

Syromyatnikov, V. G., Menelle, A., Toperverg, B. P., Soroko, Z. N. and Schebetov, A. F. 1999, *Physica B* **267–268**, 190.

Szytula, A., Kolenda, M., Troc, R., Tran, V. H., Bonet, M. and Rossat-Mignod, J. 1992, *Solid State Commun.* **81**, 481.

Tasset, F., Brown, P. J., Lelièvre-Berna, E., Roberts, T., Pujol, S., Allibon, J. and Bourgeat-Lami, E. 1999, *Physica B* **267–268**, 69.

Taylor, J. W., Smith, T. J., Anderson, K. H., Capellmann, H., Kremer, R. K., Simon, A., Schärpf, O., Neumann, K. U. and Ziebeck, K. R. A. 1999, *Eur. Phys. J. B* **12**, 199.

Watson, R. E. and Freeman, A. J. 1961, *J. Acta Crystallogr.* **14**, 27.

Wicksted, J. P., Böni, P. and Shirane, G. 1984, *Phys. Rev. B* **30**, 3655.

Williams, W. G. 1988, In *Polarized Neutrons*, Oxford Science, Clarendon Press, Oxford.

Ziebeck, K. R. A. and Brown, P. J. 1980, *J. Phys. F: Metal Phys.* **10**, 2015.